

Final Report

Emission source region contributions to a high surface ozone episode during DISCOVER-AQ

AQRP Project 14-004

Submitted to:

Gary McGaughey
Project Manager
Texas Air Quality Research Program

and

Doug Boyer
TCEQ Project Liaison

Prepared by:

Dr. Christopher P. Loughner
Earth System Science Interdisciplinary Center
University Of Maryland
5825 University Research Court, Suite 4001
College Park, MD 20740

and

Dr. Melanie Follette-Cook
Morgan State University
NASA Goddard Space Flight Center, Code 614
Greenbelt, MD 20771

QA Requirements: Audits of Data Quality: 10% Required

ACKNOWLEDGMENT

The preparation of this report was funded by a grant from the Texas Air Quality Research Program (AQRP) at The University of Texas at Austin through the Texas Emission Reduction Program (TERP) and the Texas Commission on Environmental Quality (TCEQ). The findings, opinions and conclusions are the work of the author(s) and do not necessarily represent findings, opinions, or conclusions of the AQRP or the TCEQ. We would like to acknowledge Rob Gilliam at the U.S. Environmental Protection Agency (EPA) for providing guidance in running WRF using the EPA iterative technique. We would also like to acknowledge Jim MacKay at the Texas Commission on Environmental Quality (TCEQ) for providing the TCEQ anthropogenic emissions inventory.

TABLE OF CONTENTS

ACKNOWLEDGMENT	i
EXECUTIVE SUMMARY	1
1.0 INTRODUCTION.....	2
1.1 Background.....	2
1.2 Objectives	3
1.3 Report Organization.....	3
2.0 METEOROLOGICAL AND AIR QUALITY MODELING	4
2.1 Original WRF Simulation.....	7
2.2 Improved WRF and CMAQ Simulations	10
2.3 Statistical Analysis of WRF and CMAQ Simulations.....	20
3.0 BACK TRAJECTORIES.....	27
4.0 SOURCE APPORTIONMENT CMAQ SIMULATION	29
5.0 SATELLITE ANALYSIS.....	36
6.0 AUDITS OF DATA QUALITY.....	43
7.0 CONCLUSIONS AND RECOMMENDATIONS.....	43
7.1 Summary.....	43
7.2 Recommendations.....	44
8.0 REFERENCES.....	45

Figures

Figure 1. HYSPLIT back trajectories calculated from La Porte Sylvan Beach at 2000 UTC (2:00 PM CST) September 24, 25, and 26.	3
Figure 2. 36, 12, and 4 km CMAQ modeling domains.....	4

Figure 3. 4 and 1 km CMAQ modeling domains. The red dots show the NASA P-3B aircraft spiral locations.	5
Figure 4. Observed (left) and original 4 km WRF diagnosed (right) 2 m temperature and 10 m wind velocity at 21 UTC 24 September 2013.....	8
Figure 5. Observed (left) and original 4 km WRF diagnosed (right) 2 m temperature and 10 m wind velocity at 12 UTC 25 September 2013.....	8
Figure 6. Observed (left) and original 4 km WRF diagnosed (right) 2 m temperature and 10 m wind velocity at 21 UTC 25 September 2013.....	9
Figure 7. Observed (left) and original 4 km WRF diagnosed (right) 2 m temperature and 10 m wind velocity at 12 UTC 26 September 2013.....	9
Figure 8. Observed (left) and original 4 km WRF diagnosed (right) 2 m temperature and 10 m wind velocity at 21 UTC 26 September 2013.....	10
Figure 9. Observed (left) and 4 km 2 nd iterative WRF diagnosed (right) 2 m temperature and 10 m wind velocity at 21 UTC 24 September 2013.....	12
Figure 10. Observed (left) and improved 4 km CMAQ simulated (right) maximum 8 hour average ozone on 24 September 2013.	13
Figure 11. Observed (left) and 4 km 2 nd iterative WRF diagnosed (right) 2 m temperature and 10 m wind velocity at 12 UTC 25 September 2013.....	13
Figure 12. Observed (left) and 4 km 2 nd iterative WRF diagnosed (right) 2 m temperature and 10 m wind velocity at 21 UTC 25 September 2013.....	14
Figure 13. Observed (left), improved 4 km CMAQ simulated (middle), and original 4 km CMAQ simulated (right) maximum 8 hour average ozone on 25 September 2013.	14
Figure 14. Observed (left) and 4 km 2 nd iterative WRF diagnosed (right) 2 m temperature and 10 m wind velocity at 12 UTC 26 September 2013.....	15
Figure 15. Observed (left) and 4 km 2 nd iterative WRF diagnosed (right) 2 m temperature and 10 m wind velocity at 21 UTC 26 September 2013.....	15
Figure 16. Observed (left) and improved 4 km CMAQ simulated (right) maximum 8 hour average ozone on 26 September 2013.	16
Figure 17. Location of Conroe, La Porte Sylvan Beach (LP), Bayland Place, and Park Place (PP) used in timeseries analysis.	16
Figure 18. Timeseries of 2 m temperature biases at Conroe (top left), La Porte Sylvan Beach (top right), Bayfront Place (bottom left), and Park Place (bottom right) for the original 4 km simulation, first iterative 4 and 1 km simulations, and second iterative 4 and 1 km simulations. 17	

Figure 19. Timeseries of 10 m wind speed biases at Conroe (top left), La Porte Sylvan Beach (top right), Bayfront Place (bottom left), and Park Place (bottom right) for the original 4 km simulation, first iterative 4 and 1 km simulations, and second iterative 4 and 1 km simulations. 18

Figure 20. Timeseries of 10 m wind direction biases at Conroe (top left), La Porte Sylvan Beach (top right), Bayfront Place (bottom left), and Park Place (bottom right) for the original 4 km simulation, first iterative 4 and 1 km simulations, and second iterative 4 and 1 km simulations. 19

Figure 21. Timeseries of surface ozone biases at Conroe (top left), La Porte Sylvan Beach (top right), Bayfront Place (bottom left), and Park Place (bottom right) for the original 4 km simulation and the second iterative 4 and 1 km simulations. 20

Figure 22. 24 hour back trajectories from 4 km WRF output initialized at 2 pm CST September 25 over La Porte Sylvan Beach at 0.5 km (red), 1.0 km (green), and 2.0 km (blue) AGL. Black dot shows the location of La Porte Sylvan Beach and the letter D shows the location of Dallas, TX. Trajectories pass over Dallas / Ft Worth area..... 28

Figure 23. 33 hour back trajectories from 4 km WRF output initialized at 2 pm CST September 26 over La Porte Sylvan Beach at 0.5 km (red), 1.0 km (green), and 2.0 km (blue) AGL. Black dot shows the location of La Porte Sylvan Beach and the letter B shows the location of Beaumont, TX Trajectories show recirculation of local air and transport from the Beaumont / Port Arthur area. Back trajectories were extended out to 33 hours to show recirculation of air from the Houston metropolitan area and possible transport from Beaumont, TX..... 29

Figure 24. 4 km CMAQ domain showing the five anthropogenic source regions specified in the ozone source apportionment simulation (D=Dallas; H=Houston; B=Beaumont; L=Lake Charles; M=marine; O=other). 31

Figure 25. Amount of ozone that contributed to the maximum 8 hour average ozone on September 25, 2013 from anthropogenic emissions in the Houston source region (left) and boundary conditions (right)..... 32

Figure 26. Amount of ozone that contributed to the maximum 8 hour average ozone on September 25, 2013 from anthropogenic emissions in the Beaumont source region (left) and Lake Charles source region (right). 32

Figure 27. Amount of ozone that contributed to the maximum 8 hour average ozone on September 25, 2013 from anthropogenic emissions in the Dallas source region (left) and Marine source region (right)..... 33

Figure 28. Amount of ozone that contributed to the maximum 8 hour average ozone on September 25, 2013 from anthropogenic emissions in the Other source region (left) and all natural sources (i.e., biogenic, lightning) within the 4 km domain (right). 33

Figure 29. Amount of ozone that contributed to the maximum 8 hour average ozone on September 26, 2013 from anthropogenic emissions in the Houston source region (left) and boundary conditions (right)..... 34

Figure 30. Amount of ozone that contributed to the maximum 8 hour average ozone on September 26, 2013 from anthropogenic emissions in the Beaumont source region (left) and Lake Charles source region (right).	34
Figure 31. Amount of ozone that contributed to the maximum 8 hour average ozone on September 26, 2013 from anthropogenic emissions in the Dallas source region (left) and Marine source region (right).	35
Figure 32. Amount of ozone that contributed to the maximum 8 hour average ozone on September 26, 2013 from anthropogenic emissions in the Other source region (left) and all natural sources (i.e., biogenic, lightning) within the 4 km domain (right).	35
Figure 33. OMI total ozone column on September 24, 2013.	37
Figure 34. OMI total ozone column on September 25, 2013.	38
Figure 35. OMI total ozone column on September 26, 2013.	38
Figure 36. OMI NO ₂ tropospheric column on September 24, 2013.	39
Figure 37. OMI NO ₂ tropospheric column on September 25, 2013.	39
Figure 38. OMI NO ₂ tropospheric column on September 26, 2013.	40
Figure 39. MODIS AOD on September 24, 2013.	40
Figure 40. MODIS AOD on September 25, 2013.	41
Figure 41. MODIS AOD on September 26, 2013.	41
Figure 42. MOPITT total CO column on September 24, 2013.	42
Figure 43. MOPITT total CO column on September 25, 2013.	42
Figure 44. MOPITT total CO column on September 26, 2013.	43

Tables

Table 1. Terrain-following hydrostatic-pressure vertical coordinates (η) and the hydrostatic pressure (p_h) if surface pressure is 1013.25 mb for the original and improved simulations at the edges of each grid cell.....	6
Table 2. WRF model options that were used in both the original and improved modeling scenarios.....	7
Table 3. CMAQ model options used in this study.....	11
Table 4. Definition of the statistics calculated in Tables 4-8. In these equations M represents the model results, O represents the observations, and N is the number of data points.....	21
Table 5. Mean bias (MB), normalized mean bias (NMB), normalized mean error (NME), root mean square error (RMSE), and Gross Error (GE) of 2 m temperature from the original 4 km WRF simulation and 1 st and 2 nd iterations of the 4 and 1 km WRF simulations for September 24-26. Benchmarks are from Emery et al. (2001).....	22
Table 6. MB, NMB, NME, RMSE, and GE of 10 m wind speed from the original 4 km WRF simulation and 1 st and 2 nd iterations of the 4 and 1 km WRF simulations for September 24-26. Benchmarks are from Emery et al. (2001).....	22
Table 7. MB, NMB, NME, RMSE, and GE of 10 m wind direction from the original 4 km WRF simulation and 1 st and 2 nd iterations of the 4 and 1 km WRF simulations for September 24-26. Benchmarks are from Emery et al. (2001).....	23
Table 8. MB, NMB, NME, RMSE, GE of surface ozone concentrations from the original 4 km WRF simulation and the 2 nd iterative 4 and 1 km CMAQ simulations for September 24-26.	23
Table 9. Mean bias of planetary boundary layer (PBL), free troposphere (FT), and all (PBL+FT) in-situ concentrations of O ₃ with respect to the original 4 km CMAQ simulation and the 2nd iterative 4 and 1 km CMAQ simulations for September 24-26. Boundary layer heights were obtained from the WRF output. Units are ppbv.....	24
Table 10. Mean bias of planetary boundary layer (PBL), free troposphere (FT), and all (PBL+FT) in-situ concentrations of CO with respect the 2nd iterative 4 and 1 km CMAQ simulations for September 24-26. Boundary layer heights were obtained from the WRF output. Units are ppbv.	24
Table 11. Mean bias of planetary boundary layer (PBL), free troposphere (FT), and all (PBL+FT) in-situ concentrations of HCHO with respect the 2nd iterative 4 and 1 km CMAQ simulations for September 24-26. Boundary layer heights were obtained from the WRF output. Units are ppbv.	24
Table 12. Mean bias of planetary boundary layer (PBL), free troposphere (FT), and all (PBL+FT) in-situ concentrations of NO ₂ with respect to the 2 nd iterative 4 and 1 km CMAQ	

simulations for September 24-26. Boundary layer heights were obtained from the WRF output. Units are ppbv.	25
Table 13. MB, NMB, NME, RMSE, and GE of 2 m temperature at Conroe, Bayfront Place, Park Place, and La Porte Sylvan Beach from the 2 nd iterations of the 4 km WRF simulation for September 24-26.	25
Table 14. MB, NMB, NME, RMSE, and GE of 10 m wind speed at Conroe, Bayfront Place, Park Place, and La Porte Sylvan Beach from the 2 nd iterations of the 4 km WRF simulation for September 24-26.	26
Table 15. MB, NMB, NME, RMSE, and GE of 10 m wind direction at Conroe, Bayfront Place, Park Place, and La Porte Sylvan Beach from the 2 nd iterations of the 4 km WRF simulation for September 24-26.	26
Table 16. MB, NMB, NME, RMSE, and GE of surface ozone at Conroe, Bayfront Place, Park Place, and La Porte Sylvan Beach from the 2 nd iterations of the 4 km WRF simulation for September 24-26.	27
Table 17. Observed and model simulated maximum 8 hour average ozone, contribution of maximum 8 hour average ozone (absolute value followed by percent contribution to model simulated amount in parentheses) from anthropogenic emissions in the Houston, Dallas, Beaumont, Lake Charles, Marine, and Other source regions, natural emissions throughout the 4 km domain, boundary conditions, and initial conditions at La Porte Sylvan Beach on September 25 and 26, 2013.....	36
Table 18. Same as Table 17, but for Conroe.....	36
Table 19. Same as Table 17, but for Park Place.	36
Table 20. Same as Table 17, but for Bayland Park.....	36

EXECUTIVE SUMMARY

The highest ozone air pollution episode in the Houston, TX region in 2013 occurred September 25-26, which coincided with the Deriving Information on Surface Conditions and Vertically Resolved Observations Relevant to Air Quality (DISCOVER-AQ) field campaign. The maximum 8-hour average ozone peaked on September 25 at La Porte Sylvan Beach reaching 124 ppbv, almost 50 ppbv above the current Environmental Protection Agency (EPA) standard of 75 ppbv. We analyzed this air pollution episode and have quantified the contributions of emissions from various anthropogenic source regions.

We used the Weather Research and Forecasting (WRF) and the Community Multi-scale Air Quality (CMAQ) models along with ground and aircraft observations obtained during the DISCOVER-AQ field deployment to evaluate the model simulations. Our first WRF simulation did not perform well as compared with observations (details described in Section 2.1). The WRF simulation did not accurately capture the sea and bay breeze circulations on September 25. We re-ran WRF using refined model inputs and employing a novel iterative technique developed at the EPA (details described in Section 2.2). This new and improved simulation accurately simulated the sea and bay breeze circulations on September 25. This improved WRF simulation was used to drive a CMAQ simulation. The improved CMAQ run simulated a widespread area that exceeded the EPA ozone standard, which agrees with observations. However, the model still had a low ozone bias downwind of Baytown and Deer Park. This low bias may be due to an underestimate in emissions, errors in the meteorological simulation, or uncertainties in the chemistry.

We identified possible anthropogenic source regions that impacted Houston during this campaign by calculating back trajectories from our WRF simulation. Houston, Dallas, Beaumont, Lake Charles, marine, and other areas were the anthropogenic source regions tagged for a CMAQ ozone source apportionment simulation based on the back trajectory analysis. Results from the ozone source apportionment model run show anthropogenic emissions from the Houston metropolitan area were the primary contributors to surface ozone during this air pollution episode.

Satellite observations were analyzed to determine if they were able to detect the regional transport of air pollution and subsequent buildup in the Houston metropolitan area for this air pollution episode. While satellite observations were not able to detect transport from a specific anthropogenic source region during this episode, tropospheric nitrogen dioxide (NO₂) columns and total carbon monoxide (CO) columns as observed from space did show higher pollution over the continent than over the Gulf of Mexico. This suggests that higher air pollution concentrations are transported into Houston when transport is from the continent than from the Gulf of Mexico, which was the case during this air pollution episode.

1.0 INTRODUCTION

1.1 Background

The goal of this study is to quantify the contributions of local versus regional sources to Houston's highest ozone air pollution episode in 2013 during the Deriving Information on Surface conditions from Column and Vertically Resolved Observations Relevant to Air Quality (DISCOVER-AQ) field campaign. We broke down the contribution of anthropogenic emissions in specific source regions to ozone concentrations in Houston. Previous research has shown sea breeze circulations are a critical ingredient to poor air quality in Houston (Banta et al., 2005; Chen et al., 2011; Darby, 2005; Parrish et al., 2009). Sea breeze circulations were a daily occurrence during the DISCOVER-AQ field campaign. Recent research has shown regionally transported air pollution into Houston is at its greatest concentrations when the air originates from Louisiana and the Midwest (Estes et al., 2013; Smith et al., 2013). During the September 24-26 air pollution episode, Houston may have been influenced by transport from the north. Back trajectories calculated by the Hybrid Single Particle Lagrangian Integrated Trajectory (HYSPLIT) model reveal that Houston may have experienced transport from the Gulf of Mexico and Louisiana on September 24, northeastern Texas and the Great Plains states from Oklahoma to Wyoming on September 25, and northeastern Texas and Louisiana on September 26 (Figure 1).

The evolution of this air pollution event, which is described in the DISCOVER-AQ Outlook Reports located at <http://www-air.larc.nasa.gov/missions/discover-aq/reports.tx2013/>, is briefly summarized here. On September 24, air was transported from Louisiana and the Gulf of Mexico over the Houston metropolitan area. On the 25th, northerly flow brought continental air over Houston. High air pollution levels that were observed aloft in the residual layer in the morning mixed down to the surface impacting surface air quality, indicating pollution emitted on a previous day or overnight from local and/or regional sources impacted surface air quality in Houston on the 25th. In addition, a sea breeze circulation developed in the afternoon causing pollutants that were transported over the water in the morning to recirculate back inland and converge with pollutants over land at the sea breeze convergence zone. La Porte Sylvan Beach was near the sea breeze front and reported maximum 8 hr average ozone of 124 ppbv, the highest observed value in the Houston metropolitan area in 2013. On the 26th, winds were primarily from the south and southeast, resulting in maximum recorded ozone concentrations to the north and northwest of Houston (reported maximum 8 hr average ozone was 85 ppbv in Conroe, TX).

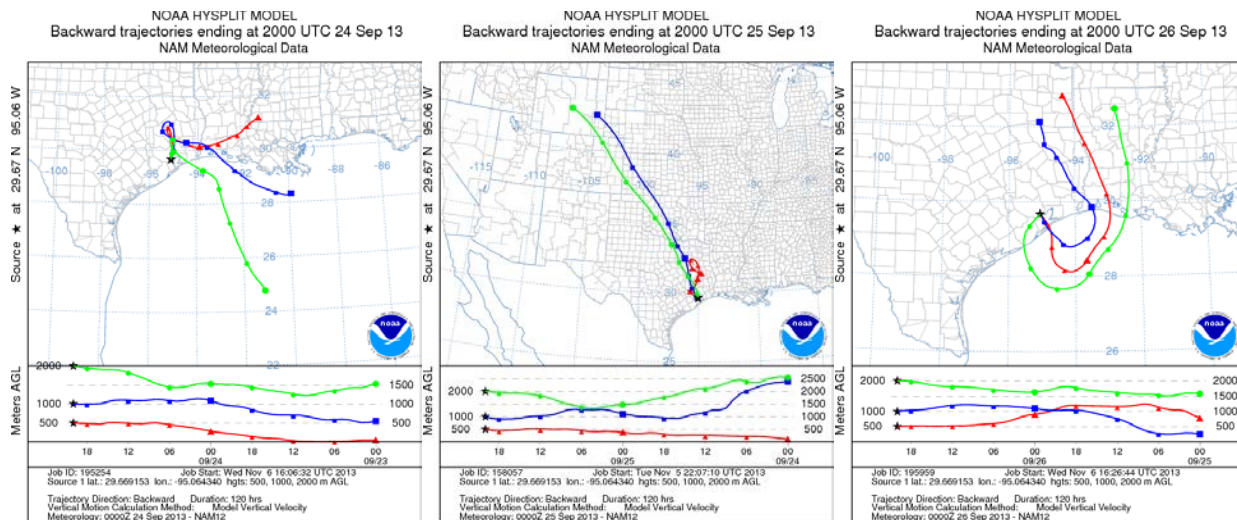


Figure 1. HYSPLIT back trajectories calculated from La Porte Sylvan Beach at 2000 UTC (2:00 PM CST) September 24, 25, and 26.

1.2 Objectives

The goal of this study is to quantify the contributions of local versus regional sources to Houston's highest ozone air pollution episode in 2013 during the DISCOVER-AQ field campaign. We will break down the contribution of emissions in specific source regions to ozone concentrations in Houston.

1.3 Report Organization

Section 2 describes two sets of WRF and CMAQ model simulations performed in this study. Section 3 presents the back trajectories performed in order to locate anthropogenic source regions for the source apportionment CMAQ simulation, which is described in Section 4. Section 5 shows whether satellites observed regional transport of pollutants into the Houston region during this air pollution event. Audits of data quality are described in Section 6. Our conclusions and recommendations are presented in Section 7.

2.0 METEOROLOGICAL AND AIR QUALITY MODELING

Two sets of WRF model simulations were performed from August 18, 2013 through October 1, 2013. This time period covers the entire DISCOVER-AQ Texas field deployment in September 2013 plus additional days in August to provide adequate model spin-up time. The original simulation, described in detail in Section 2.1, did not adequately simulate the sea and bay breezes that contributed to the surface ozone episode on September 25. Improved WRF and CMAQ runs, described in Section 2.2, captured the meteorological and air quality representation of this ozone episode. The 36, 12, and 4 km modeling domains used in this study are shown in Figure 2. In addition, the improved CMAQ simulation included a 1 km simulation, which is shown in Figure 3. This project primarily uses model output from the 4 km domain. All WRF and CMAQ simulations employ 45 vertical levels, with the original simulation extending from the surface to 100 mb and the improved simulation extending from the surface to 50 mb (Table 1). A statistical analysis comparing the original 4 km simulation and improved 4 and 1 km simulations are described in Section 2.3. WRF options that are used in both the original and improved simulations are shown in Table 2. The WRF simulation employed observational nudging of the National Centers for Environmental Prediction (NCEP) Automated Data Processing (ADP) Global Surface (<http://rda.ucar.edu/datasets/ds461.0/>) and Upper Air (<http://rda.ucar.edu/datasets/ds351.0/>) Observational Weather Data. The WRF simulation also utilized the Multi-scale Ultra-high Resolution (MUR) Sea Surface Temperature (SST) Analysis, which has a horizontal resolution of about 1 km (available at: http://podaac.jpl.nasa.gov/Multi-scale_Ultra-high_Resolution_MUR-SST).

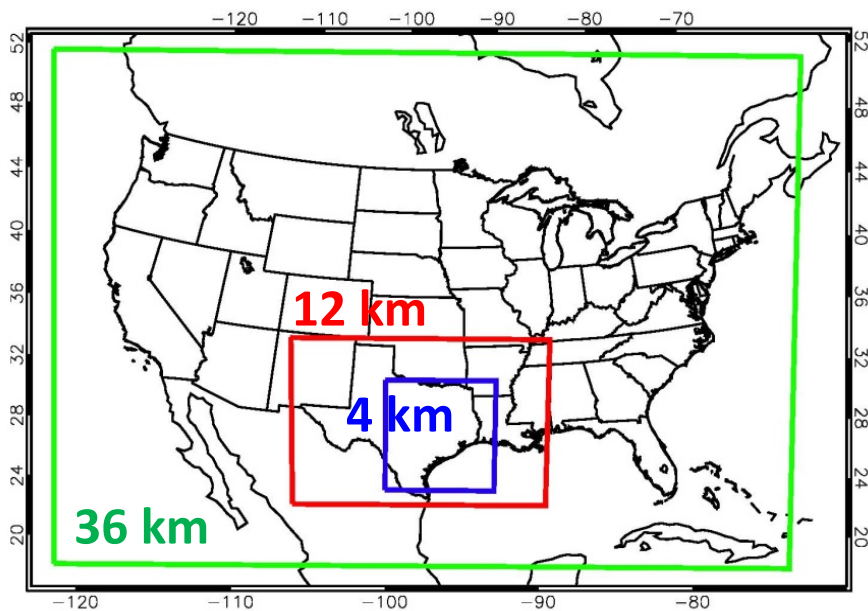


Figure 2. 36, 12, and 4 km CMAQ modeling domains.

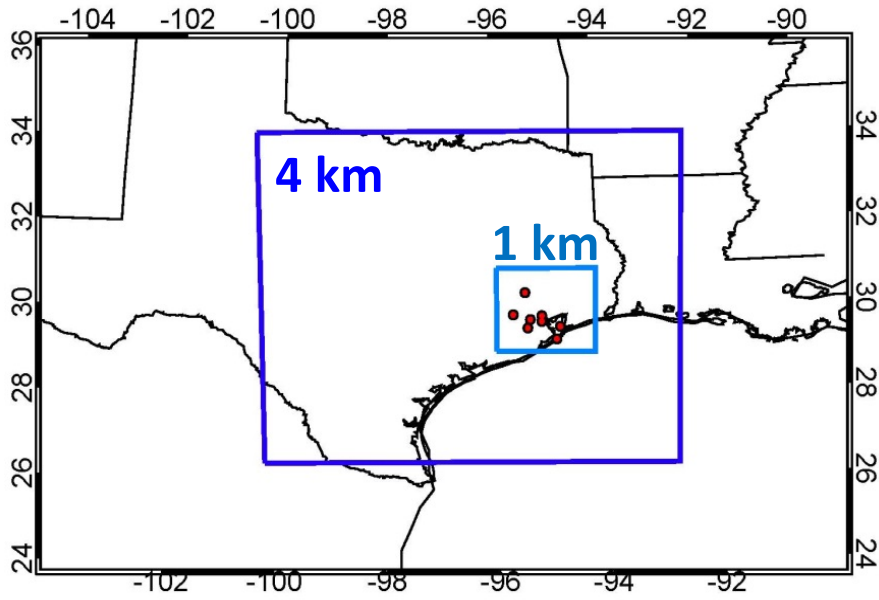


Figure 3. 4 and 1 km CMAQ modeling domains. The red dots show the NASA P-3B aircraft spiral locations.

Original				Improved			
η	p_h	η	p_h	η	p_h	η	p_h
1	1013.25	0.572206	622.567	1	1013.25	0.594721	622.865
0.997256	1010.74	0.536611	590.06	0.9974	1010.75	0.561	590.383
0.993667	1007.47	0.500683	557.249	0.994	1007.47	0.526963	557.597
0.989444	1003.61	0.464533	524.235	0.99	1003.62	0.492715	524.608
0.984589	999.176	0.42825	491.099	0.9854	999.187	0.458342	491.498
0.978467	993.585	0.392211	458.187	0.9796	993.6	0.4242	458.611
0.970761	986.547	0.356505	425.578	0.9723	986.568	0.390373	426.027
0.961472	978.064	0.321464	393.577	0.9635	978.091	0.357176	394.05
0.950178	967.75	0.286978	362.083	0.9528	967.785	0.324505	362.579
0.936772	955.507	0.253378	331.397	0.9401	955.551	0.292674	331.918
0.921044	941.143	0.221221	302.03	0.9252	941.199	0.262209	302.573
0.902783	924.467	0.191281	274.687	0.9079	924.535	0.233845	275.251
0.881989	905.476	0.16378	249.572	0.8882	905.559	0.207792	250.156
0.85845	883.979	0.139163	227.091	0.8659	884.078	0.18447	227.691
0.832167	859.977	0.116874	206.735	0.841	860.093	0.163354	207.351
0.810728	840.397	0.096803	188.406	0.82069	840.53	0.14	184.855
0.788329	819.941	0.078839	172	0.79947	820.089	0.12	165.59
0.76349	797.257	0.062317	156.911	0.775938	797.422	0.1	146.325
0.736211	772.345	0.046903	142.835	0.750095	772.529	0.083	129.95
0.706493	745.205	0.032044	129.264	0.721941	745.41	0.07	117.427
0.674778	716.241	0.017851	116.302	0.691895	716.468	0.052632	100.697
0.641401	685.759	0.0041	103.745	0.660275	686.01	0.03	78.8975
0.607247	654.568	0	100	0.627918	654.842	0	50

Table 1. Terrain-following hydrostatic-pressure vertical coordinates (η) and the hydrostatic pressure (p_h) if surface pressure is 1013.25 mb for the original and improved simulations at the edges of each grid cell.

Weather Research and Forecasting (WRF) Version 3.6.1 Model Options	
Radiation	Long Wave: Rapid Radiative Transfer Model (RRTM) Short Wave: Goddard
Surface Layer	Pleim-Xiu
Land Surface Model	Pleim-Xiu
Boundary Layer	Asymmetric Convective Model (ACM2)
Cumulus	Kain-Fritsch
Microphysics	WRF Single-Moment 6 (WSM-6)
Nudging	Observational and analysis nudging
Damping	Vertical velocity and gravity waves damped at top of modeling domain
SSTs	Multi-scale Ultra-high Resolution (MUR) SST analysis (~1 km resolution)

Table 2. WRF model options that were used in both the original and improved modeling scenarios.

2.1 Original WRF Simulation

The original WRF simulation used the North American Regional Reanalysis (NARR), which has a horizontal resolution of 40 km, for initial and boundary conditions. WRF was re-initialized every 3 days and run in 3.5 day increments, with the first 12 hours discarded for each model run. Observational and analysis nudging were performed only on the 36 km domain. WRF and model output fields were saved hourly.

For September 24, one of the two cleanest days during the month long campaign, WRF diagnosed 2 m temperatures and 10 m wind velocities are in agreement with the observations (Figure 4).

On the morning of September 25, WRF simulated light winds from the northwest over Houston and westerly winds south of Houston, whereas observations showed stagnant conditions over Houston and light northwesterly winds south of Houston (Figure 5). In the afternoon, WRF simulated a weaker bay breeze than observed (Figure 6). Observed southeasterlies along the western shore of the Galveston Bay likely caused high air pollution levels over the Galveston Bay to be transported onshore resulting in peak maximum 8 hour average ozone concentrations to be located along the western shore of the Galveston Bay. However, WRF simulated northerlies near the western coastline of Galveston Bay.

For September 26, WRF simulated weak winds in the morning and overnight hours and southeasterlies in the afternoon, which is in agreement with observations (Figure 7 and Figure 8).

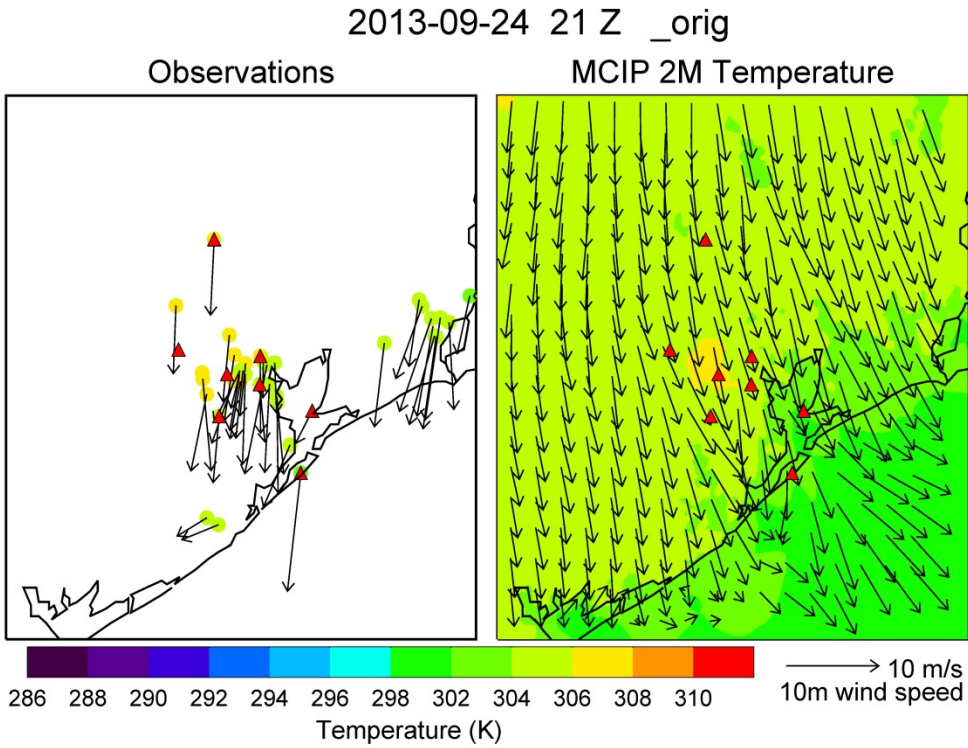


Figure 4. Observed (left) and original 4 km WRF diagnosed (right) 2 m temperature and 10 m wind velocity at 21 UTC 24 September 2013.

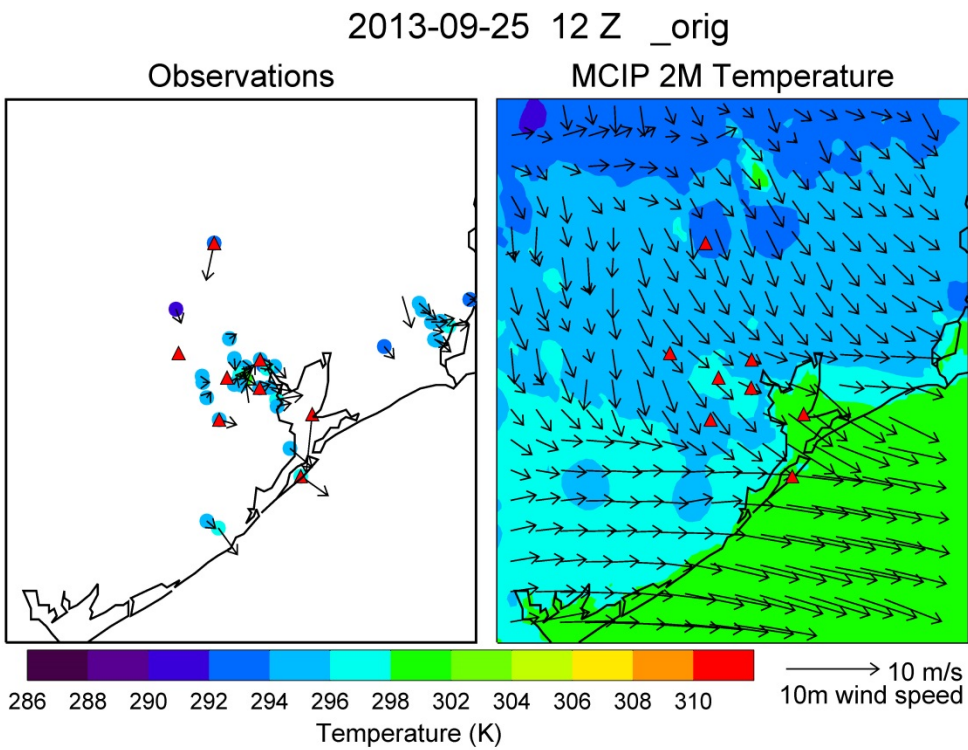


Figure 5. Observed (left) and original 4 km WRF diagnosed (right) 2 m temperature and 10 m wind velocity at 12 UTC 25 September 2013.

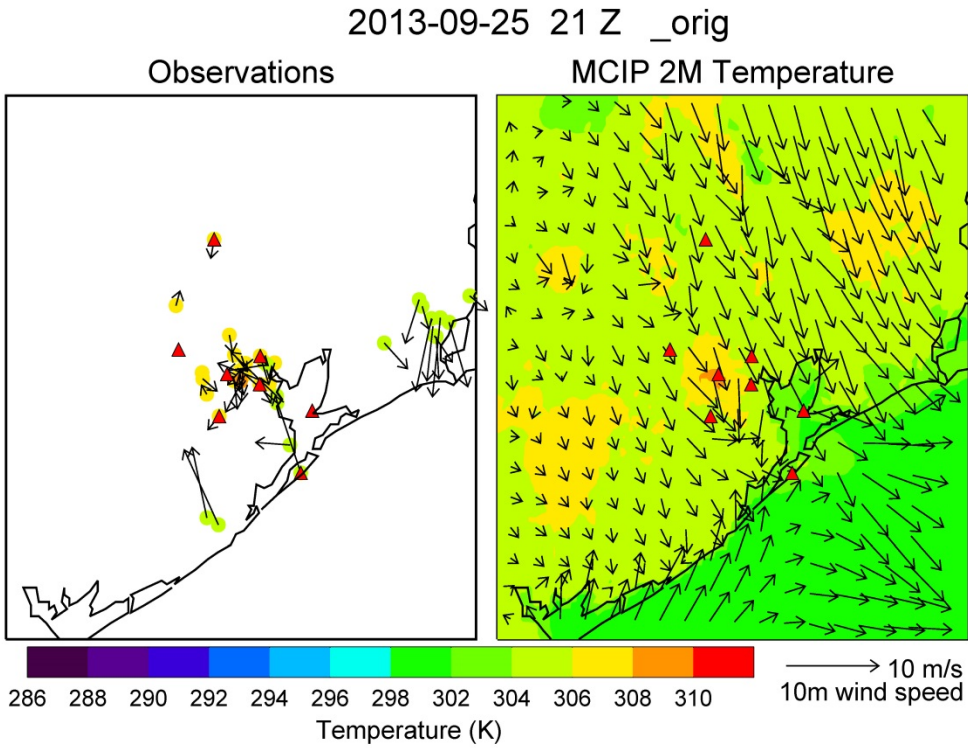


Figure 6. Observed (left) and original 4 km WRF diagnosed (right) 2 m temperature and 10 m wind velocity at 21 UTC 25 September 2013.

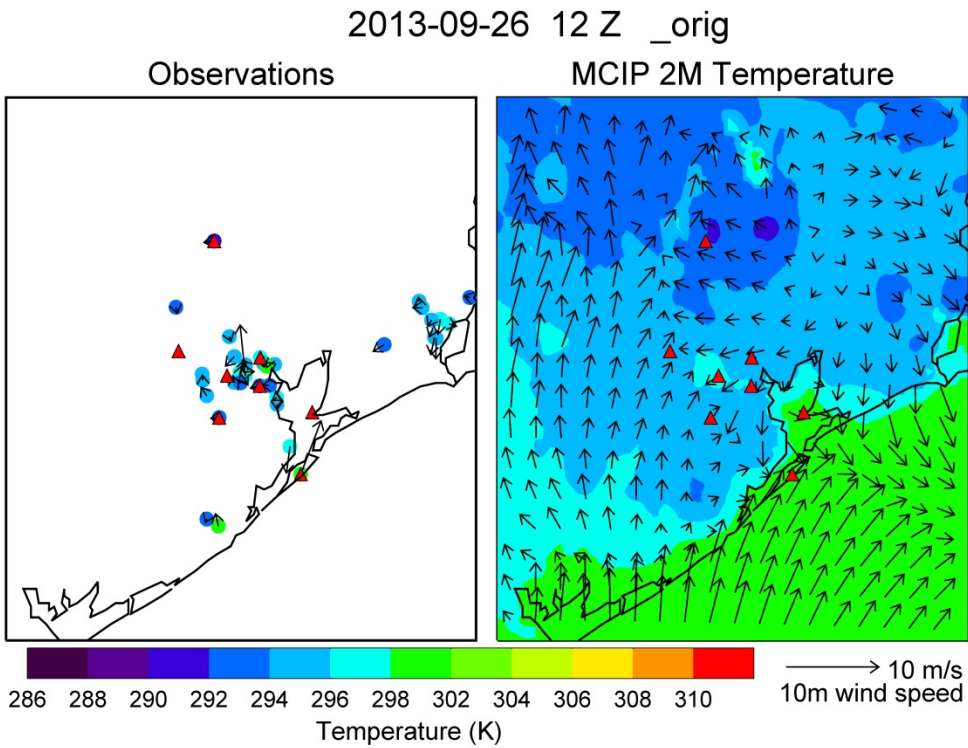


Figure 7. Observed (left) and original 4 km WRF diagnosed (right) 2 m temperature and 10 m wind velocity at 12 UTC 26 September 2013.

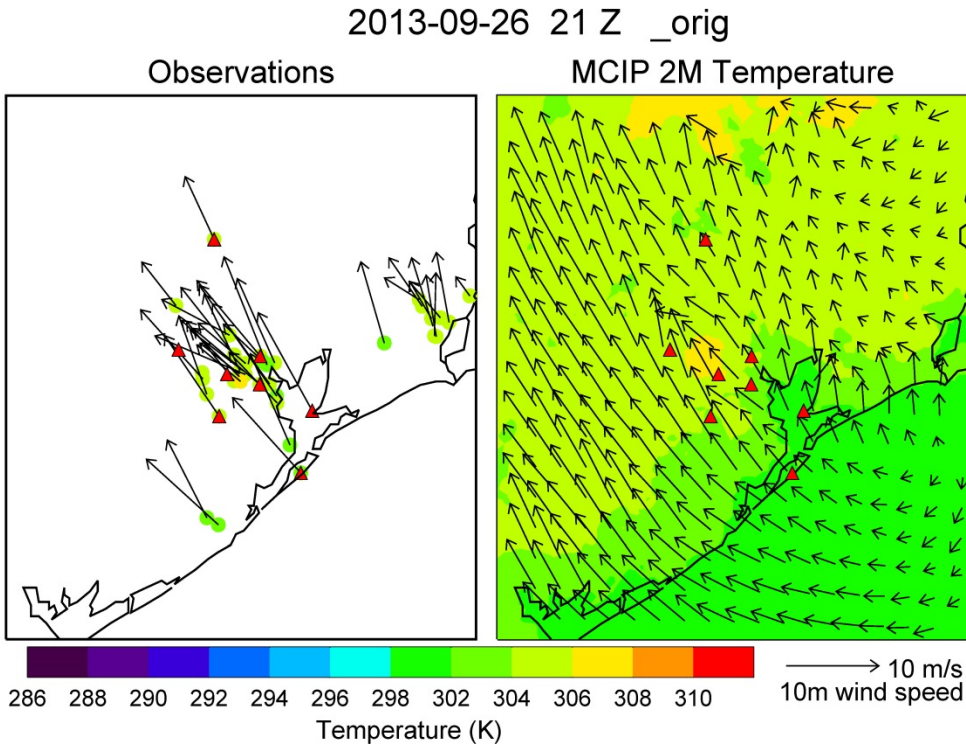


Figure 8. Observed (left) and original 4 km WRF diagnosed (right) 2 m temperature and 10 m wind velocity at 21 UTC 26 September 2013.

2.2 Improved WRF and CMAQ Simulations

The WRF modeling technique and inputs were revised to improve the representation of model simulated sea and bay breezes and the air pollution episode. The 12 km North American Mesoscale (NAM) model was used for meteorological initial and boundary conditions instead of the NARR, which has a horizontal resolution of 40 km. Observational and analysis nudging were performed on all domains, whereas the original WRF simulation only nudged the 36 km domain. In addition, a 1 km modeling domain was included. This project primarily used output from the 4 km domain in order to include areas outside of the 1 km domain in the ozone source apportionment simulation. Project #14-002 used output from the 1 km domain. Model output was saved hourly for the 36 and 12 km domains, every 20 minutes for the 4 km domain, and every 5 minutes for the 1 km domain. The WRF model was output at higher temporal resolutions than hourly to prevent the output to be smoothed temporally. CMAQ was run to ingest the meteorology on the same temporal resolution as the WRF model output.

WRF was run straight through (i.e., was not re-initialized at all) using an iterative technique developed at the EPA. The EPA successfully used the WRF iterative technique to simulate the meteorology and air quality during the DISCOVER-AQ Maryland campaign. Like Houston, Maryland air quality is affected by bay breeze circulations. A description of improvements and benefits to the WRF-CMAQ system by the EPA, including a description of the WRF iterative technique, is described in Appel et al. (2014). The iterative technique involved running WRF twice. The first WRF run performed analysis nudging on all domains based on the 12 km NAM. The second WRF run performed analysis nudging on all domains based on the 12 km NAM

except for 2 m temperature and humidity for the 4 and 1 km domains. 2 m temperature and humidity from 4 and 1 km 1st WRF iterative run was used to nudge the 2nd WRF iterative 4 and 1 km domains. This modeling technique prevented the relatively coarse NAM 12 km model from degrading the high resolution WRF modeling domains (4 and 1 km modeling domains). The 2nd iterative WRF runs were used to drive the improved CMAQ simulations. CMAQ model options are shown in Table 3. Statistics from both WRF simulations and the CMAQ simulations are discussed in Section 2.3.

CMAQ Version 5.0.2 Model Options	
Chemical Mechanism	Carbon Bond (CB05)
Aerosol Module	Aerosols with aqueous extensions version 5 (AE5)
Dry deposition	M3DRY
Vertical diffusion	Asymmetric Convective Model 2 (ACM2)
Emissions	2012 TCEQ anthropogenic emissions Biogenic Emission Inventory System (BEIS) calculated within CMAQ
Initial and Boundary conditions	Model for Ozone and Related chemical Tracers (MOZART) Chemical Transport Model (CTM)

Table 3. CMAQ model options used in this study.

For September 24, WRF diagnosed 2 m temperatures and 10 m wind velocities and CMAQ simulated maximum 8 hour average ozone are in agreement with observations (Figure 9 and Figure 10).

On the morning of September 25, WRF simulated light winds from the northwest and observations reveal stagnant conditions over Houston (Figure 11). In the afternoon, the new WRF simulation significantly improved the representation of the sea and bay breezes with the sea and bay breeze fronts pushing farther inland (Figure 12) compared to the original WRF simulation (Figure 6). Observed and simulated maximum 8 hour average ozone is shown in Figure 13. A high model bias is present at Galveston, which may be due to the lack of halogen chemistry that would result in ozone destruction over the Gulf of Mexico (Sarwar et al., 2015). In addition, CMAQ has lower ozone concentrations along the coastline of the bay. This may be due to a low estimate in emissions, errors in the meteorology, such as less simulated stagnation in the early morning and errors in the bay breeze circulation, and/or uncertainties in the model chemistry.

For September 26, like the original simulation, the improved WRF simulation agrees with observed winds and temperature (Figure 14-15). The CMAQ simulation agrees with the observed magnitude and spatial distribution of maximum 8 hour average ozone (Figure 16).

A timeseries analysis for Conroe, La Porte Sylvan Beach, Bayfront Place, and Park Place (see Figure 17 for a map showing these locations) was performed. Timeseries plots for 2 m temperature, 10 m wind speed, 10 m wind direction, and surface ozone are shown in Figure 18-21. As can be seen from the meteorological timeseries (Figure 18-20), the 1st iterative 1 km WRF

simulation performed poorly. This is due to nudging the model with the relatively coarse 12 km NAM degrading the model. The 2nd iterative 1 and 4 km simulations performed the best, as will be shown statistically in the next section. The timeseries at La Porte Sylvan Beach (Figure 21 top right) shows the low ozone bias on September 25.

Since the updated WRF model simulation was run with different inputs, configuration, and methodology, we cannot determine how each individual change impacted the WRF simulation. Future WRF simulations changing one aspect of how WRF is run at a time would be beneficial to determine the optimal inputs, configuration and methodology for running WRF for the Houston region.

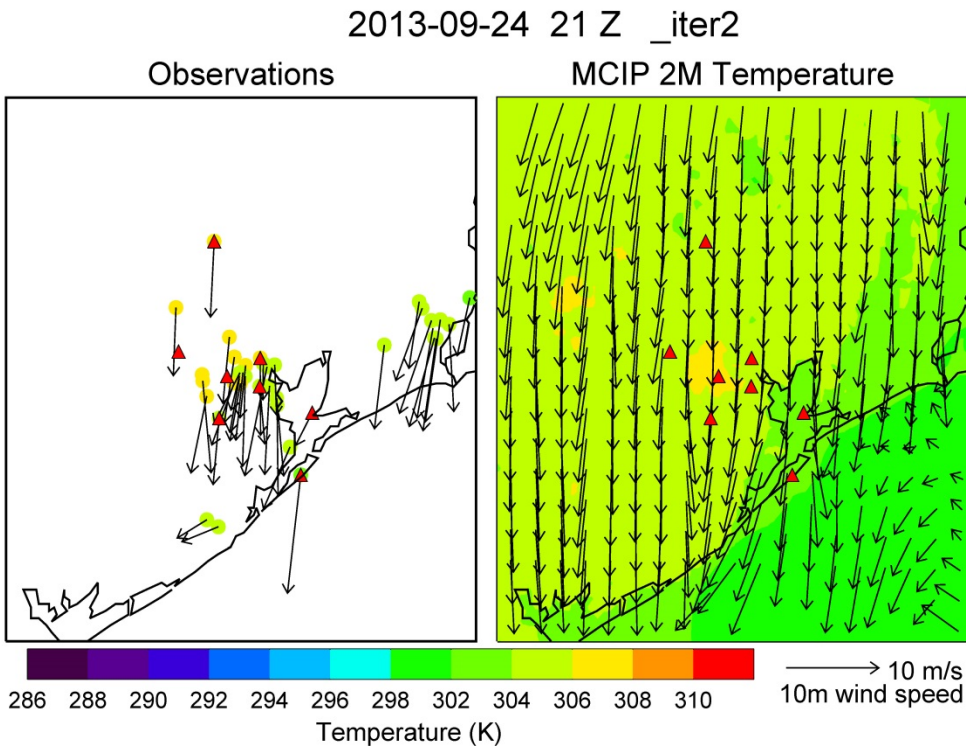


Figure 9. Observed (left) and 4 km 2nd iterative WRF diagnosed (right) 2 m temperature and 10 m wind velocity at 21 UTC 24 September 2013.

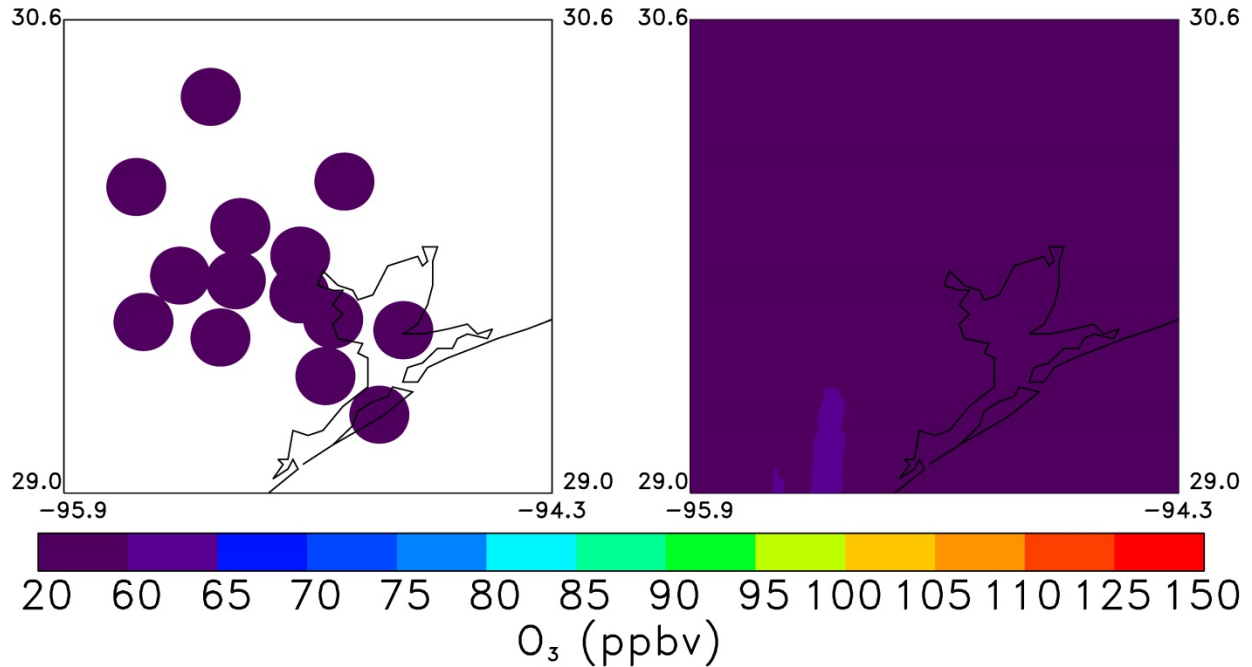


Figure 10. Observed (left) and improved 4 km CMAQ simulated (right) maximum 8 hour average ozone on 24 September 2013.

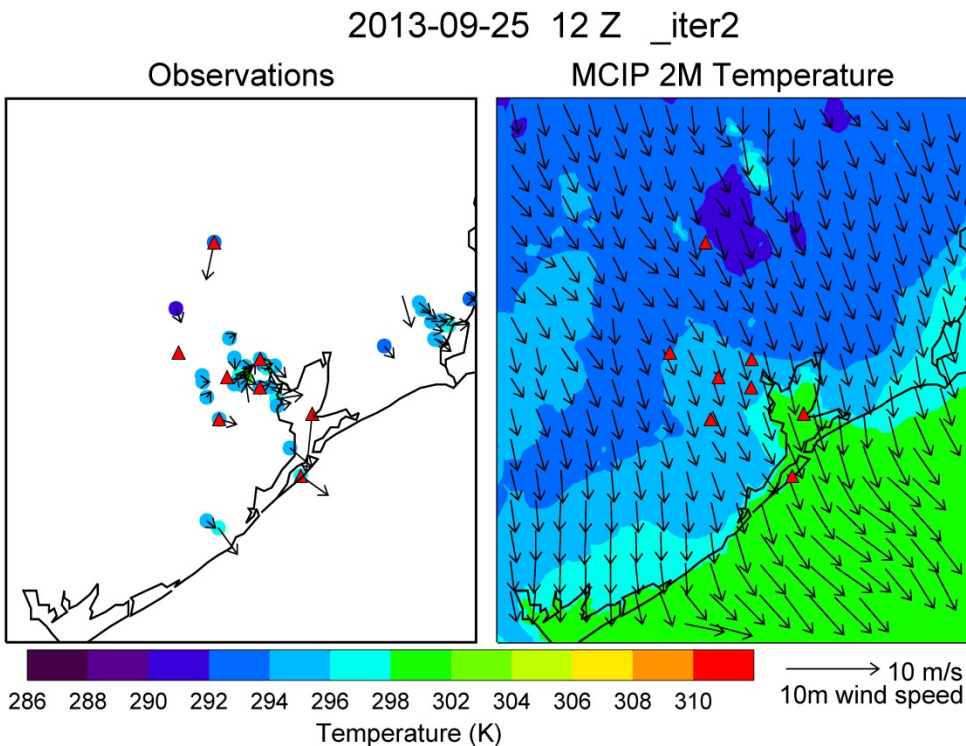


Figure 11. Observed (left) and 4 km 2nd iterative WRF diagnosed (right) 2 m temperature and 10 m wind velocity at 12 UTC 25 September 2013.

2013-09-25 21 Z _iter2

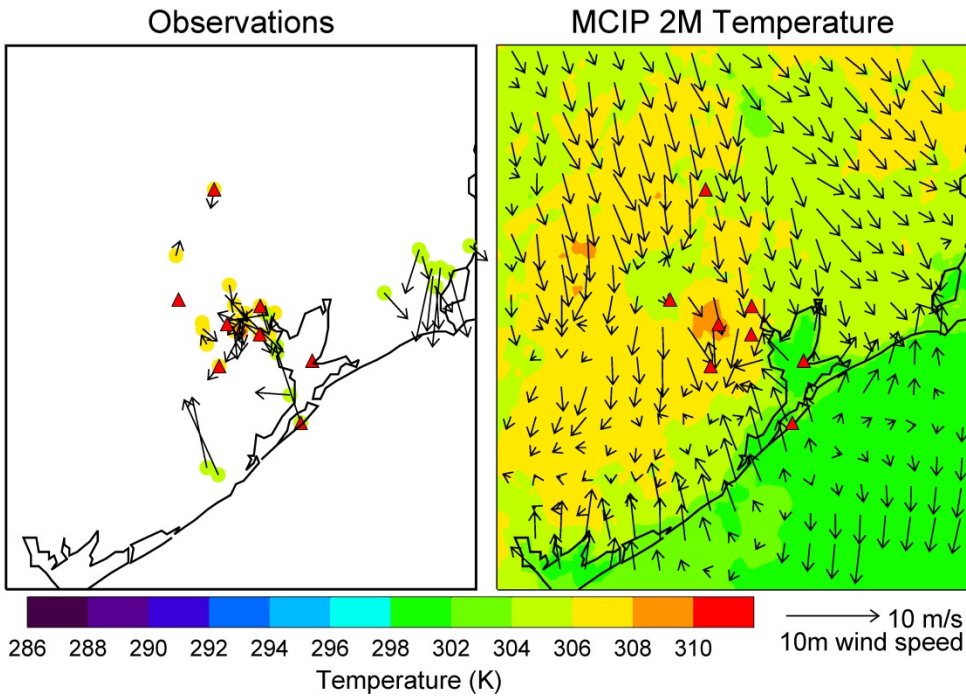


Figure 12. Observed (left) and 4 km 2nd iterative WRF diagnosed (right) 2 m temperature and 10 m wind velocity at 21 UTC 25 September 2013.

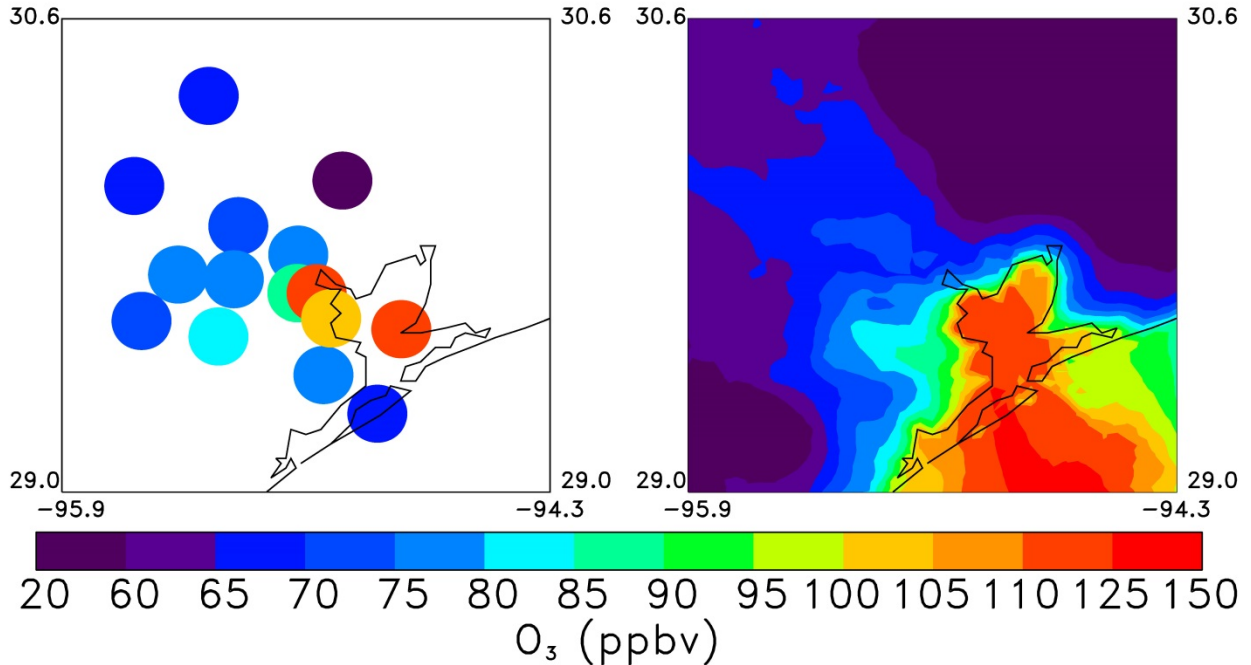


Figure 13. Observed (left), improved 4 km CMAQ simulated (middle), and original 4 km CMAQ simulated (right) maximum 8 hour average ozone on 25 September 2013.

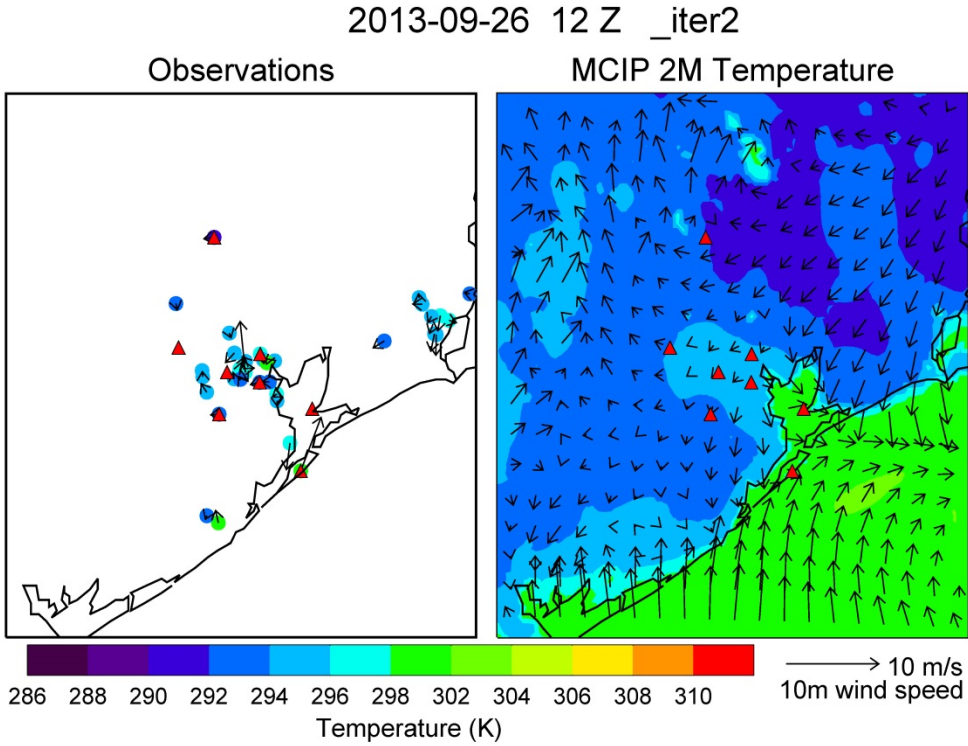


Figure 14. Observed (left) and 4 km 2nd iterative WRF diagnosed (right) 2 m temperature and 10 m wind velocity at 12 UTC 26 September 2013.

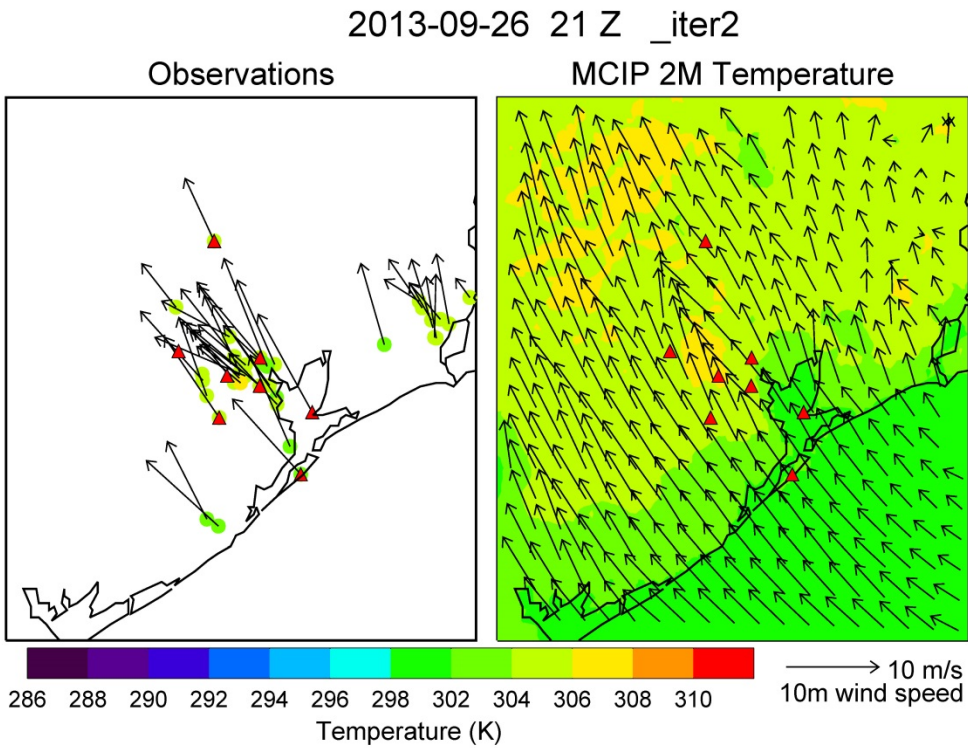


Figure 15. Observed (left) and 4 km 2nd iterative WRF diagnosed (right) 2 m temperature and 10 m wind velocity at 21 UTC 26 September 2013.

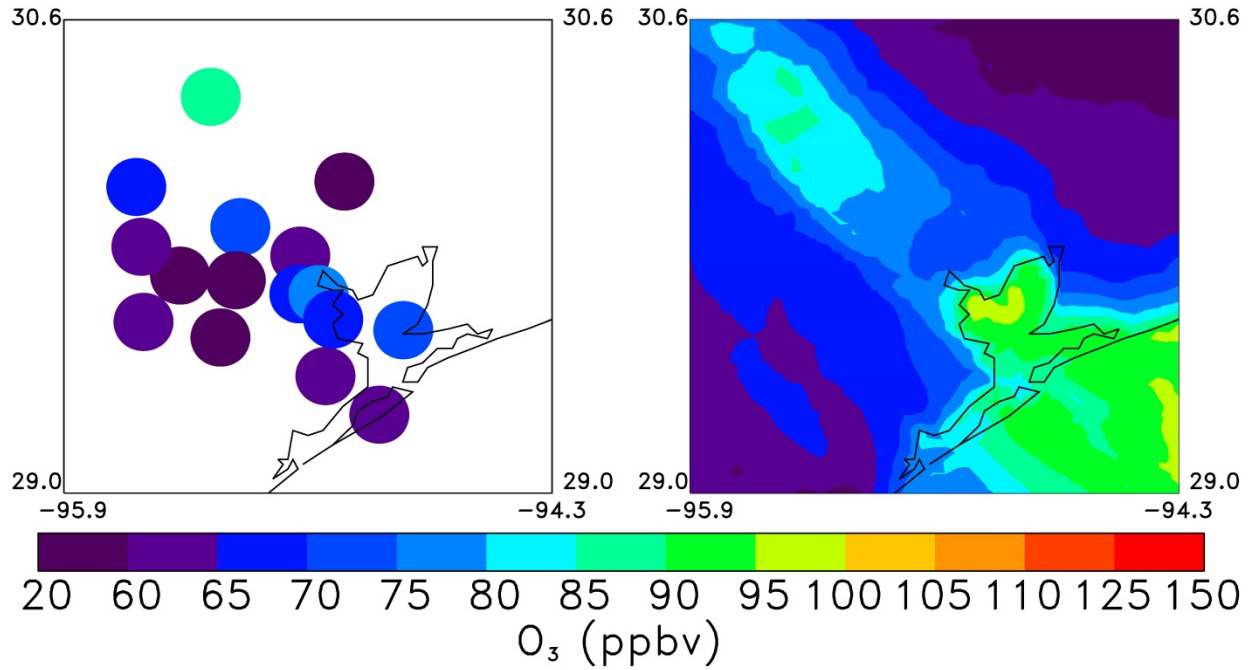


Figure 16. Observed (left) and improved 4 km CMAQ simulated (right) maximum 8 hour average ozone on 26 September 2013.

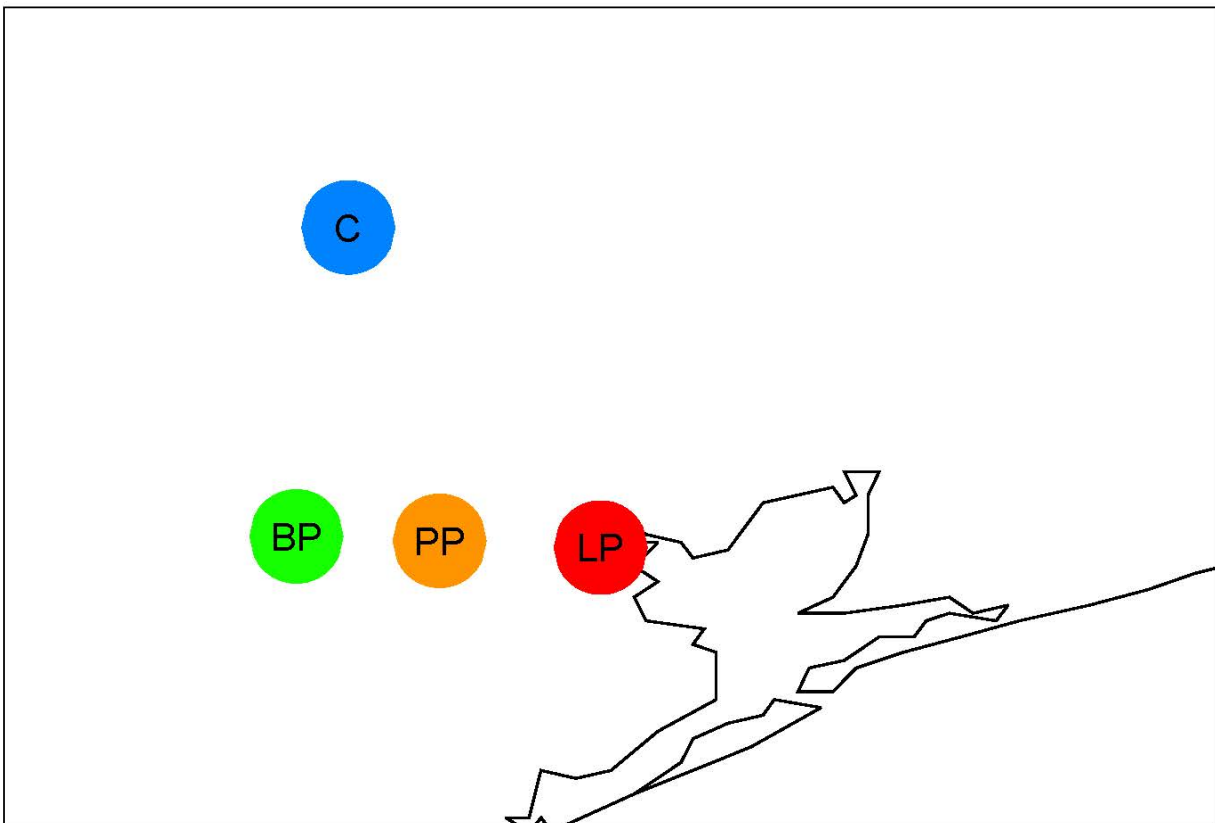


Figure 17. Location of Conroe, La Porte Sylvan Beach (LP), Bayland Place, and Park Place (PP) used in timeseries analysis.

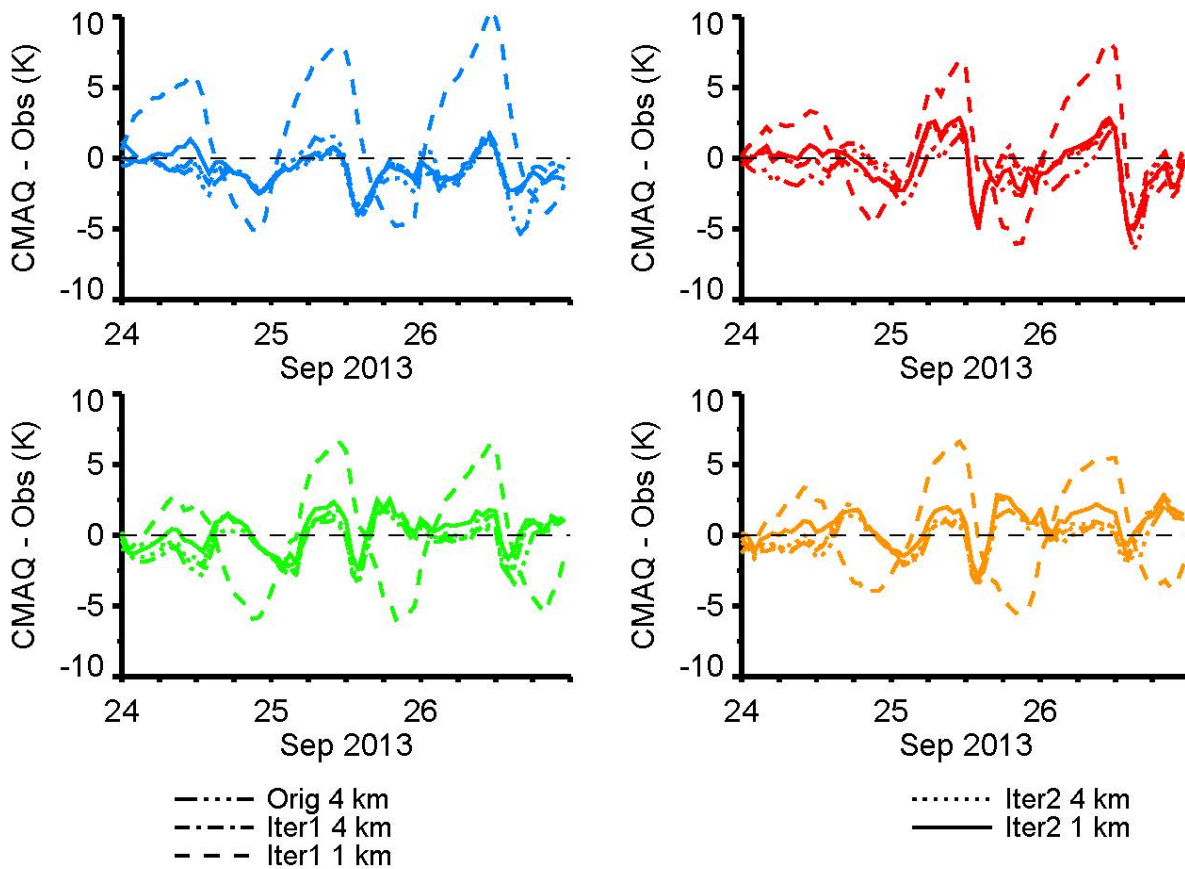


Figure 18. Timeseries of 2 m temperature biases at Conroe (top left), La Porte Sylvan Beach (top right), Bayfront Place (bottom left), and Park Place (bottom right) for the original 4 km simulation, first iterative 4 and 1 km simulations, and second iterative 4 and 1 km simulations.

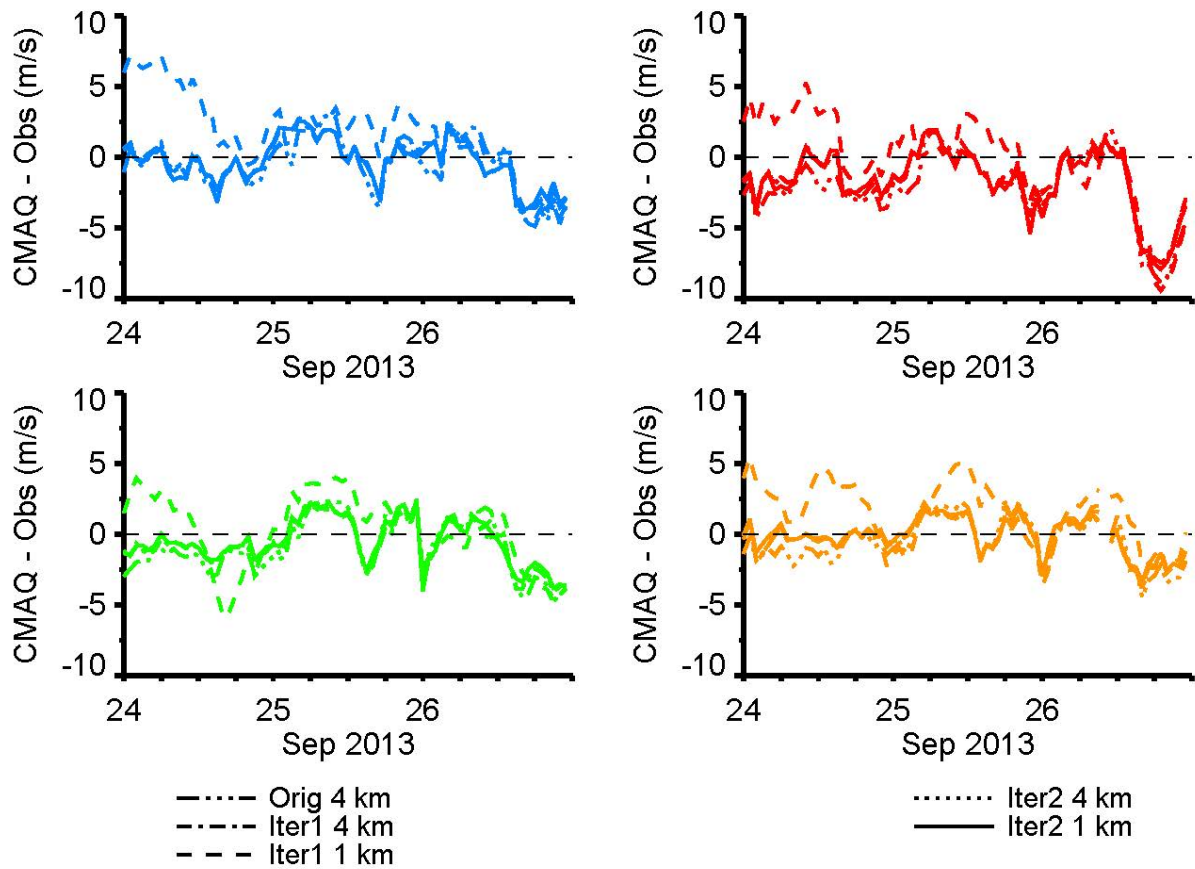


Figure 19. Timeseries of 10 m wind speed biases at Conroe (top left), La Porte Sylvan Beach (top right), Bayfront Place (bottom left), and Park Place (bottom right) for the original 4 km simulation, first iterative 4 and 1 km simulations, and second iterative 4 and 1 km simulations.

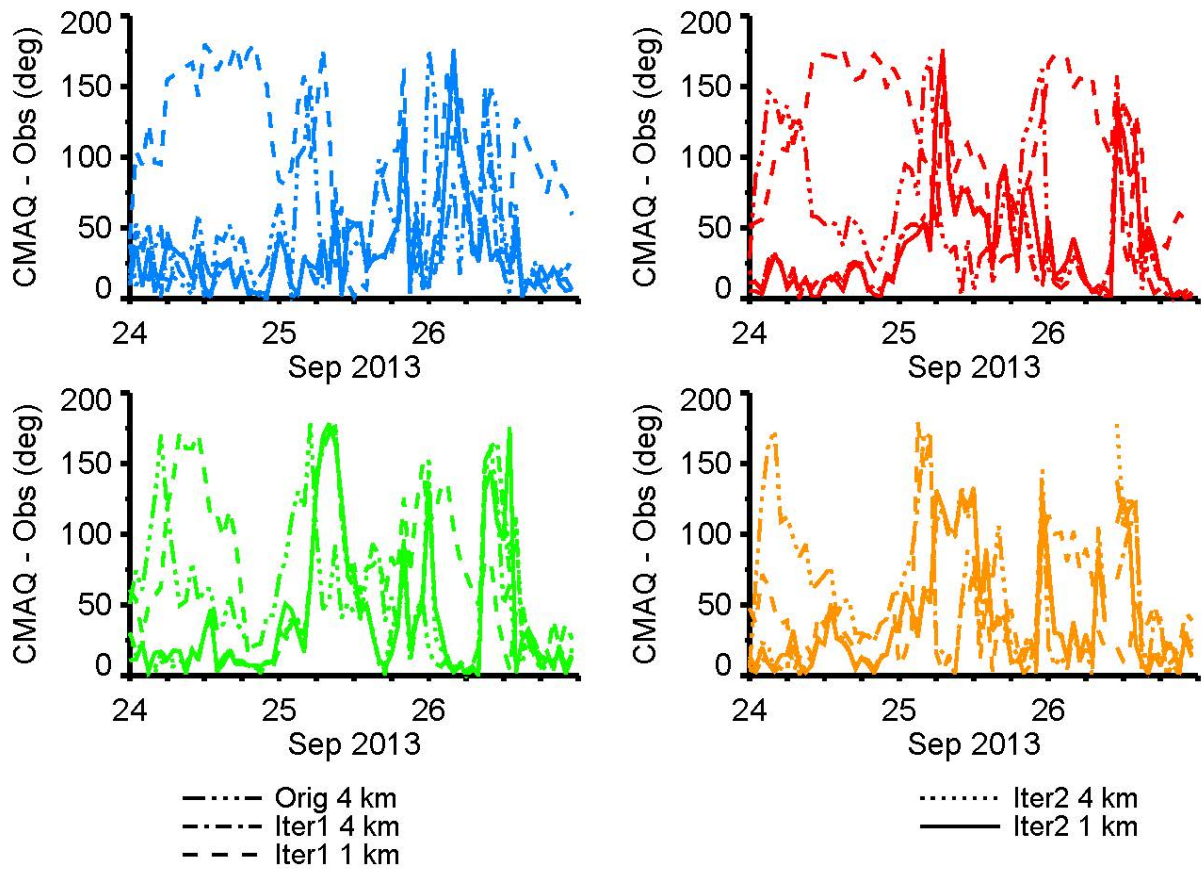


Figure 20. Timeseries of 10 m wind direction biases at Conroe (top left), La Porte Sylvan Beach (top right), Bayfront Place (bottom left), and Park Place (bottom right) for the original 4 km simulation, first iterative 4 and 1 km simulations, and second iterative 4 and 1 km simulations.

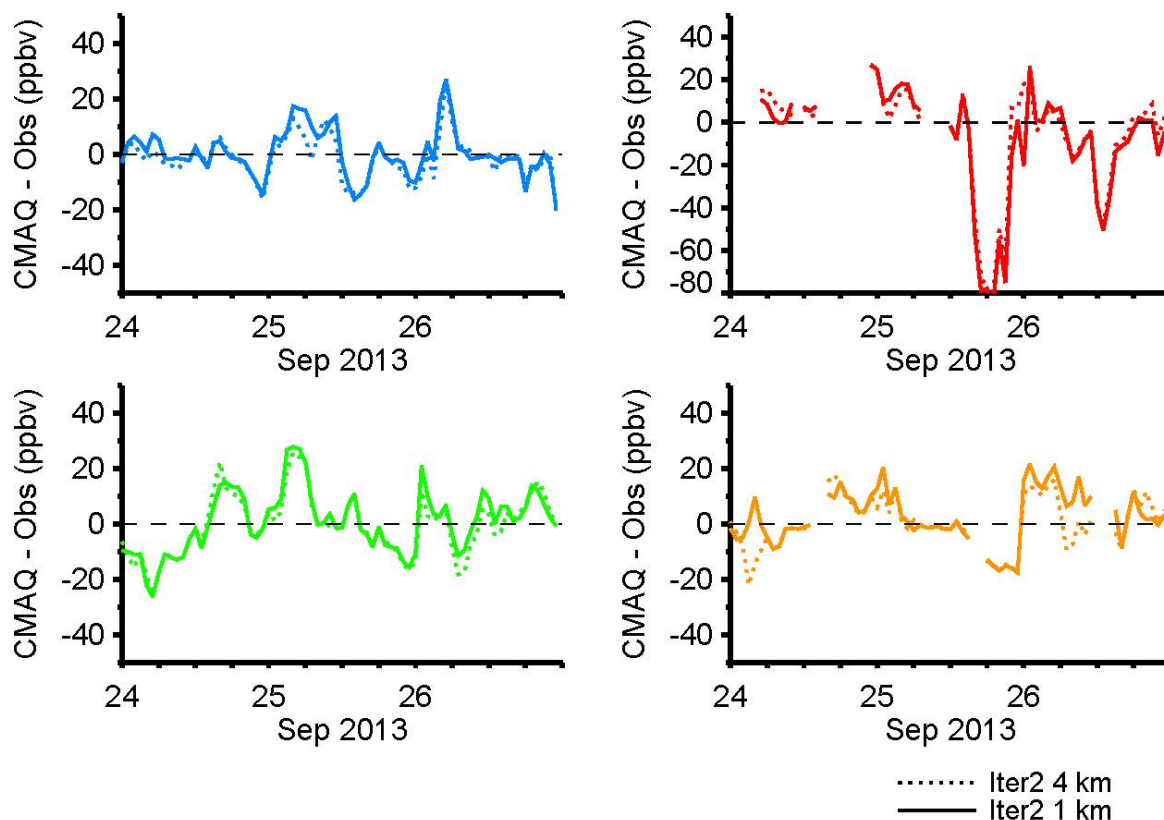


Figure 21. Timeseries of surface ozone biases at Conroe (top left), La Porte Sylvan Beach (top right), Bayfront Place (bottom left), and Park Place (bottom right) for the original 4 km simulation and the second iterative 4 and 1 km simulations.

2.3 Statistical Analysis of WRF and CMAQ Simulations

Table 4 describes the statistics used to evaluate the various WRF and CMAQ simulations.

A statistical analysis of WRF 2 m temperature, 10 m wind speed, and 10 m wind direction from our original 4 km WRF simulation and 1st and 2nd iterative 4 and 1 km WRF simulations with surface measurements at AQS sites are shown in Table 5, Table 6, and Table 7, respectively. The 2nd iterative 1 km simulation performed the best statistically for 2 m temperature and 10 m wind speed and direction. The 1st and 2nd iterative 4 km WRF simulations have similar biases and errors for temperature and winds, suggesting little improvement is gained from the expense of a 2nd iterative simulation for a 4 km domain. However, the 2nd iterative 1 km WRF simulation gained significant improvement over the 1st iterative 1 km run. The 1st iterative 1 km simulation performed the worst out of the 5 simulations analyzed for wind speed and direction. The original 4 km simulation performed worse than the 1st and 2nd iterative 4 km simulations for temperature and wind speed and direction.

A statistical analysis of CMAQ ozone concentrations for the 2nd iterative 4 and 1 km simulations compared with surface AQS sites and airborne in-situ observations are shown in Table 8 and Table 9, respectively. The 2nd iterative 4 and 1 km simulations were statistically similar. The comparisons with surface observations seen in Table 8 show that the simulations performed similarly. Model-observations statistics of CO, HCHO, and NO₂ using measurements made onboard the NASA P-3B aircraft during all flight days are shown in Table 10 through Table 12.

A statistical analysis of the four sites shown in Figure 17 (Conroe, Bayfront Place, Park Place, and La Porte Sylvan Beach) for 2 m temperature, 10 m wind speed, 10 m wind direction, and surface ozone are shown in Table 13 through Table 17. The largest ozone bias is located at La Porte Sylvan Beach, the location of the highest recorded ozone on September 25. A low model bias in wind speed and biases in wind direction may have caused errors in ozone transport to La Porte Sylvan Beach during the complex local-scale bay breeze event.

Mean Bias (MB)	$MB = \frac{1}{N} \sum_{i=1}^N (M_i - O_i)$
Normalized Mean Bias (NMB)	$NMB = \frac{\sum_{i=1}^N (M_i - O_i)}{\sum_{i=1}^N O_i} \times 100\%$
Normalized Mean Error (NME)	$NME = \frac{\sum_{i=1}^N M_i - O_i }{\sum_{i=1}^N O_i} \times 100\%$
Root Mean-Square Error (RMSE)	$RMSE = \sqrt{\frac{1}{N} \sum_{i=1}^N (M_i - O_i)^2}$
Gross Error (G)	$GE = \frac{1}{N} \sum_{i=1}^N M_i - O_i $

Table 4. Definition of the statistics calculated in Tables 4-8. In these equations M represents the model results, O represents the observations, and N is the number of data points.

		2 m Temperature (K)				
	Bench mark	Original (4km)	Iterative 1 (4 km)	Iterative 1 (1 km)	Iterative 2 (4 km)	Iterative 2 (1 km)
MB	$\leq \pm 0.5$ K	-0.8	-0.5	0.6	-0.5	-0.1
NMB (%)		-0.2	-0.2	0.2	-0.2	-0.04
NME (%)		0.4	0.4	1.0	0.4	0.4
RMSE		1.6	1.4	3.6	1.5	1.4
GE	$\leq \pm 2$ K	1.3	1.1	3.0	1.1	1.1

Table 5. Mean bias (MB), normalized mean bias (NMB), normalized mean error (NME), root mean square error (RMSE), and Gross Error (GE) of 2 m temperature from the original 4 km WRF simulation and 1st and 2nd iterations of the 4 and 1 km WRF simulations for September 24-26. Benchmarks are from Emery et al. (2001).

		10 m Wind Speed (m/s)				
	Bench mark	Original (4km)	Iterative 1 (4 km)	Iterative 1 (1 km)	Iterative 2 (4 km)	Iterative 2 (1 km)
MB	$\leq \pm 0.5$ m/s	-0.8	-0.5	1.0	-0.5	-0.4
NMB (%)		-21	-14	28	14	-12
NME (%)		50	42	70	42	43
RMSE	≤ 2 m/s	2.2	1.9	2.9	1.9	1.9
GE		1.7	1.4	2.4	1.5	1.5

Table 6. MB, NMB, NME, RMSE, and GE of 10 m wind speed from the original 4 km WRF simulation and 1st and 2nd iterations of the 4 and 1 km WRF simulations for September 24-26. Benchmarks are from Emery et al. (2001).

		10 m Wind Direction (deg)				
	Bench mark	Original (4km)	Iterative 1 (4 km)	Iterative 1 (1 km)	Iterative 2 (4 km)	Iterative 2 (1 km)
MB	$\leq \pm 10^\circ$	56	37	70	38	38
NMB (%)		39	26	49	26	26
NME (%)		39	26	49	26	26
RMSE		73	55	88	56	55
GE	$\leq 30^\circ$	56	37	71	38	38

Table 7. MB, NMB, NME, RMSE, and GE of 10 m wind direction from the original 4 km WRF simulation and 1st and 2nd iterations of the 4 and 1 km WRF simulations for September 24-26. Benchmarks are from Emery et al. (2001).

Surface Ozone (ppbv)		
	Iterative 2 (4 km)	Iterative 2 (1 km)
MB	3.2	3.9
NMB (%)	10	12
NME (%)	30	30
RMSE	13	13
GE	9.5	9.6

Table 8. MB, NMB, NME, RMSE, GE of surface ozone concentrations from the original 4 km WRF simulation and the 2nd iterative 4 and 1 km CMAQ simulations for September 24-26.

	September 24			September 25			September 26		
	PBL+FT	PBL	FT	PBL+FT	PBL	FT	PBL+FT	PBL	FT
Iteration 2 4 km	5.2	4.4	5.9	-6.4	-12	-2.9	-3.7	-1.5	-6.3
Iteration 2 1 km	3.4	1.9	4.9	-7.0	-12	-3.8	-4.3	-2.9	-5.9

Table 9. Mean bias of planetary boundary layer (PBL), free troposphere (FT), and all (PBL+FT) in-situ concentrations of O₃ with respect to the original 4 km CMAQ simulation and the 2nd iterative 4 and 1 km CMAQ simulations for September 24-26. Boundary layer heights were obtained from the WRF output. Units are ppbv.

	September 24			September 25			September 26		
	PBL+FT	PBL	FT	PBL+FT	PBL	FT	PBL+FT	PBL	FT
Iteration 2 4 km	-1.9	-9.1	3.8	-11	-24	-3.7	7.4	4.8	10
Iteration 2 1 km	-1.4	-8.0	4.2	-12	-24	-5.9	5.6	1.0	11

Table 10. Mean bias of planetary boundary layer (PBL), free troposphere (FT), and all (PBL+FT) in-situ concentrations of CO with respect the 2nd iterative 4 and 1 km CMAQ simulations for September 24-26. Boundary layer heights were obtained from the WRF output. Units are ppbv.

	September 24			September 25			September 26		
	PBL+FT	PBL	FT	PBL+FT	PBL	FT	PBL+FT	PBL	FT
Iteration 2 4 km	-0.1	-0.2	0.04	-0.9	-1.2	-0.7	0.1	0.1	0.1
Iteration 2 1 km	-0.1	-0.3	0.1	-1.0	-1.2	-0.8	0.02	-0.1	0.1

Table 11. Mean bias of planetary boundary layer (PBL), free troposphere (FT), and all (PBL+FT) in-situ concentrations of HCHO with respect the 2nd iterative 4 and 1 km CMAQ simulations for September 24-26. Boundary layer heights were obtained from the WRF output. Units are ppbv.

	September 24			September 25			September 26		
	PBL+FT	PBL	FT	PBL+FT	PBL	FT	PBL+FT	PBL	FT
Iteration 2 4 km	-0.3	-0.5	-0.1	-0.8	-1.1	-0.6	-0.1	-0.2	-0.01
Iteration 2 1 km	-0.1	-0.2	0.01	-0.7	-0.9	-0.6	-0.1	-0.2	-0.01

Table 12. Mean bias of planetary boundary layer (PBL), free troposphere (FT), and all (PBL+FT) in-situ concentrations of NO₂ with respect to the 2nd iterative 4 and 1 km CMAQ simulations for September 24-26. Boundary layer heights were obtained from the WRF output. Units are ppbv.

	Temperature (K)			
	Conroe	Bayfront Place	Park Place	La Porte Sylvan Beach
MB	-1.0	-0.2	0.3	-0.3
NMB (%)	-0.3	-0.1	0.1	-0.1
NME (%)	0.3	0.4	0.4	0.4
RMSE	1.4	1.3	1.4	1.6
GE	1.1	1.1	1.1	1.2

Table 13. MB, NMB, NME, RMSE, and GE of 2 m temperature at Conroe, Bayfront Place, Park Place, and La Porte Sylvan Beach from the 2nd iterations of the 4 km WRF simulation for September 24-26.

	Wind Speed (m/s)			
	Conroe	Bayfront Place	Park Place	La Porte Sylvan Beach
MB	-0.3	-0.6	-0.2	-1.6
NMB (%)	-9.3	-19	-7.0	-34
NME (%)	48	40	33	41
RMSE	1.7	1.7	1.3	2.7
GE	1.3	1.4	1.0	2.0

Table 14. MB, NMB, NME, RMSE, and GE of 10 m wind speed at Conroe, Bayfront Place, Park Place, and La Porte Sylvan Beach from the 2nd iterations of the 4 km WRF simulation for September 24-26.

	Wind Direction (deg)			
	Conroe	Bayfront Place	Park Place	La Porte Sylvan Beach
MB	34	41	42	37
NMB (%)	27	27	32	31
NME (%)	27	27	32	31
RMSE	48	63	59	53
GE	34	41	42	37

Table 15. MB, NMB, NME, RMSE, and GE of 10 m wind direction at Conroe, Bayfront Place, Park Place, and La Porte Sylvan Beach from the 2nd iterations of the 4 km WRF simulation for September 24-26.

	Surface Ozone (ppbv)			
	Conroe	Bayfront Place	Park Place	La Porte Sylvan Beach
MB	-1.3	-0.3	0.4	-6.1
NMB (%)	-3.6	-1.1	1.1	-14
NME (%)	15	25	22	36
RMSE	7.7	11	9.2	26
GE	5.6	8.6	7.3	16

Table 16. MB, NMB, NME, RMSE, and GE of surface ozone at Conroe, Bayfront Place, Park Place, and La Porte Sylvan Beach from the 2nd iterations of the 4 km WRF simulation for September 24-26.

3.0 BACK TRAJECTORIES

Back trajectories calculated with the Read/Interpolate/Plot (RIP; <http://www.mmm.ucar.edu/wrf/users/docs/ripug.htm>) program from the 2nd iterative 4 km WRF model output initialized over La Porte Sylvan Beach on September 25 and 26 are shown in Figure 22 and Figure 23. For September 25 a 24 hour back trajectory shows transport from the Dallas / Ft Worth area and for September 26, a 33 hour back trajectory shows transport from the Beaumont / Port Arthur area. Based on this analysis, we identified the following anthropogenic emissions source regions to select for an ozone source apportionment simulation: 1) Houston; 2) Dallas; 3) Beaumont; 4) Lake Charles; 5) marine; and 6) other areas.

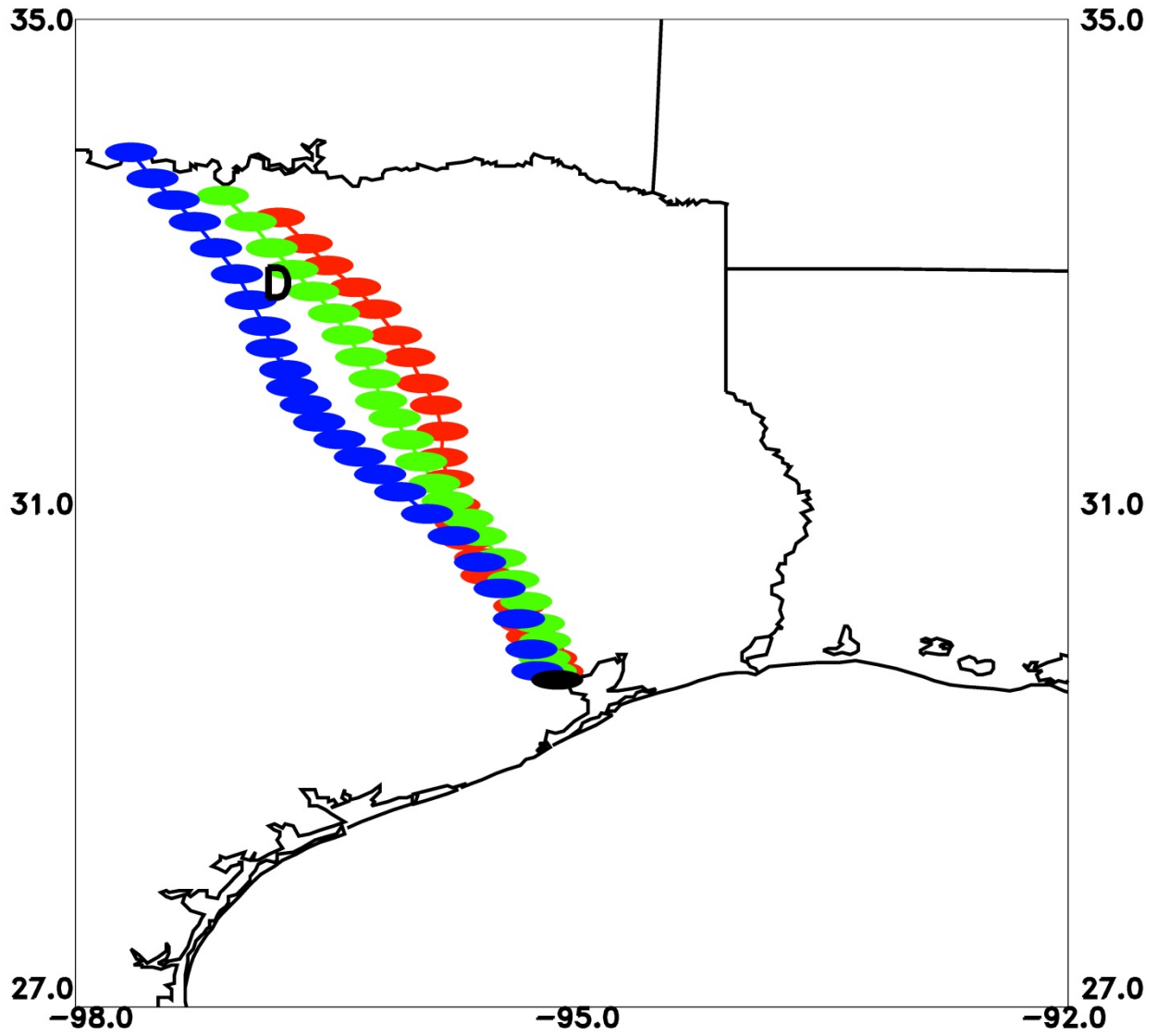


Figure 22. 24 hour back trajectories from 4 km WRF output initialized at 2 pm CST September 25 over La Porte Sylvan Beach at 0.5 km (red), 1.0 km (green), and 2.0 km (blue) AGL. Black dot shows the location of La Porte Sylvan Beach and the letter D shows the location of Dallas, TX. Trajectories pass over Dallas / Ft Worth area.

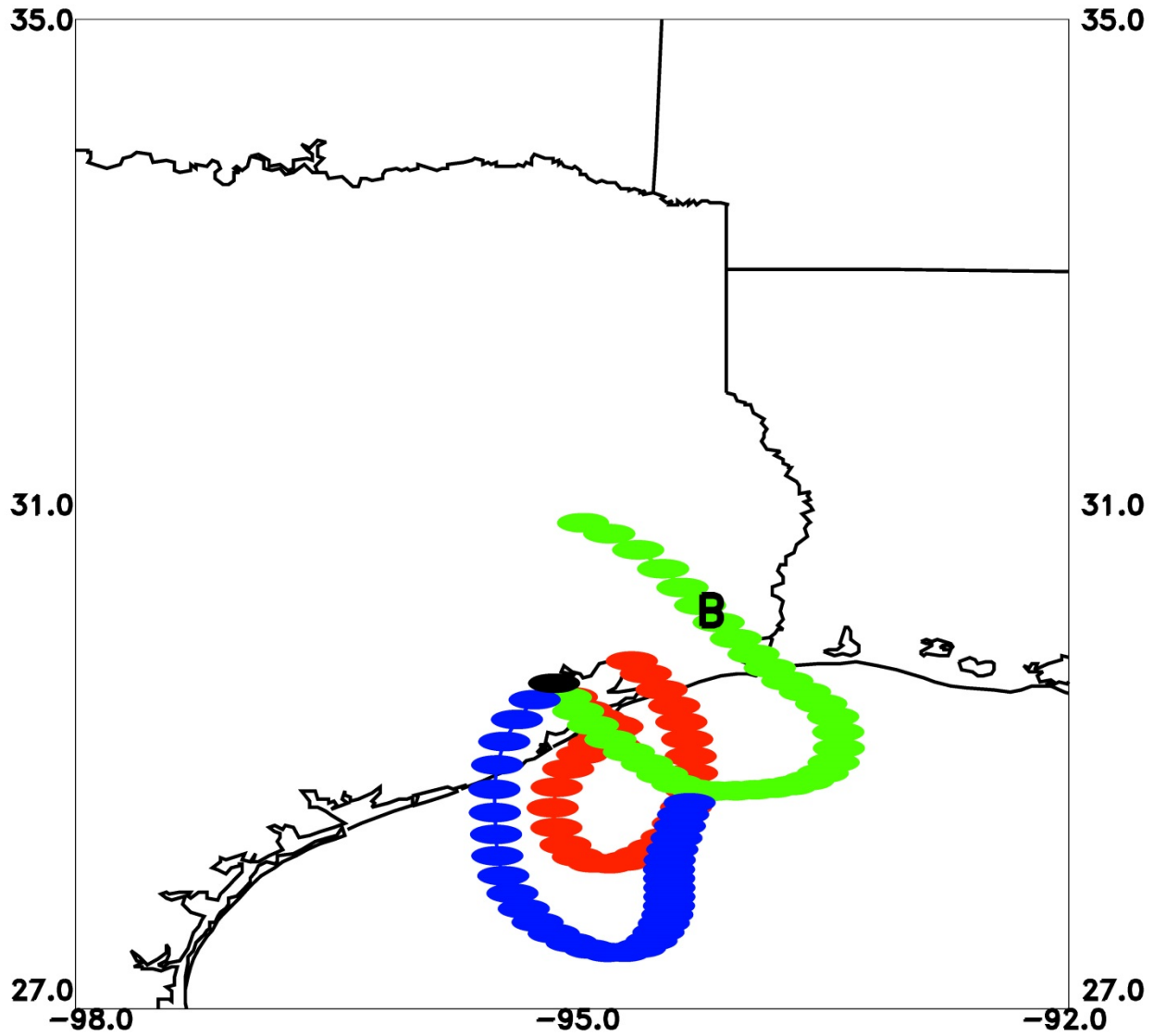


Figure 23. 33 hour back trajectories from 4 km WRF output initialized at 2 pm CST September 26 over La Porte Sylvan Beach at 0.5 km (red), 1.0 km (green), and 2.0 km (blue) AGL. Black dot shows the location of La Porte Sylvan Beach and the letter B shows the location of Beaumont, TX Trajectories show recirculation of local air and transport from the Beaumont / Port Arthur area. Back trajectories were extended out to 33 hours to show recirculation of air from the Houston metropolitan area and possible transport from Beaumont, TX.

4.0 SOURCE APPORTIONMENT CMAQ SIMULATION

A CMAQ source apportionment simulation was performed for the air pollution episode at a horizontal resolution of 4 km. Based on the back trajectory analysis, we identified the following anthropogenic source regions to perform an ozone source apportionment simulation: 1) Houston; 2) Dallas; 3) Beaumont; 4) Lake Charles; 5) marine; and 6) other areas. The anthropogenic source regions are shown in Figure 24. The CMAQ source apportionment simulation was

initialized at 0Z on September 21 to allow for almost all of the initial conditions to be transported out of the domain so they would have a minimal impact on the source apportionment outputs during the simulated air pollution event on September 25 and 26. The 4 km CMAQ output was used for the initial conditions and the only differences between the base and source apportionment outputs were the additional source apportionment outputs that describe the contribution of anthropogenic emissions source regions, initial conditions, boundary conditions, and natural emissions (biogenic, natural marine, windblown dust, and lightning) on ozone concentrations. The contribution to boundary conditions in this analysis includes all emissions outside of the 4 km domain.

The impact of emissions source regions on maximum 8 hour average ozone are shown in Figure 25 through Figure 28 for September 25, 2013 and in Figure 29 through Figure 32 for September 26, 2013. A subjective analysis of September 25, near the area of peak ozone along the western shore of Galveston Bay (Figure 25 to Figure 28), shows anthropogenic emissions from Houston contributed 45-50 ppbv, boundary conditions contributed 35-40 ppbv, anthropogenic emissions from Dallas contributed 1-3 ppbv, anthropogenic emissions from other source regions contributed 7-10 ppbv, and natural emissions (biogenic, natural marine, windblown dust, and lightning emissions) from the entire 4 km domain contributed 10-15 ppbv to the maximum 8 hour average ozone. A subjective analysis for September 26, near the peak ozone northwest of downtown Houston (Figure 29 to Figure 32), shows anthropogenic emissions from Houston contributed 25-30 ppbv, boundary conditions, which includes emissions sources outside of 4 km domain, contributed 35-40 ppbv, anthropogenic emissions from Dallas contributed 1-2 ppbv, marine emissions contributed 0-3 ppbv, anthropogenic emissions from other source regions contributed 5-7 ppbv, and natural emissions from the entire 4 km domain contributed 7-10 ppbv to the maximum 8 hour average ozone. Higher contributions from outside the region on Houston air quality is due to transport from the continent and is shown here in the boundary conditions contribution (discussed more in next section).

A comparison of the contribution of maximum 8 hour average ozone at La Porte Sylvan Beach, Conroe, Park Place, and Bayland Park are shown in Table 17 through Table 20. At La Porte Sylvan Beach, anthropogenic marine emissions had a larger impact on September 26 due to onshore winds throughout the day. At Conroe, the contribution of Dallas emissions was larger on September 25 than September 26 due to northerly transport on the September 25 and southeasterly transport on the September 26. The contribution of Houston emissions at Conroe was stronger on September 26 than September 25 due to Conroe being upwind of Houston on September 25 and downwind on September 26.

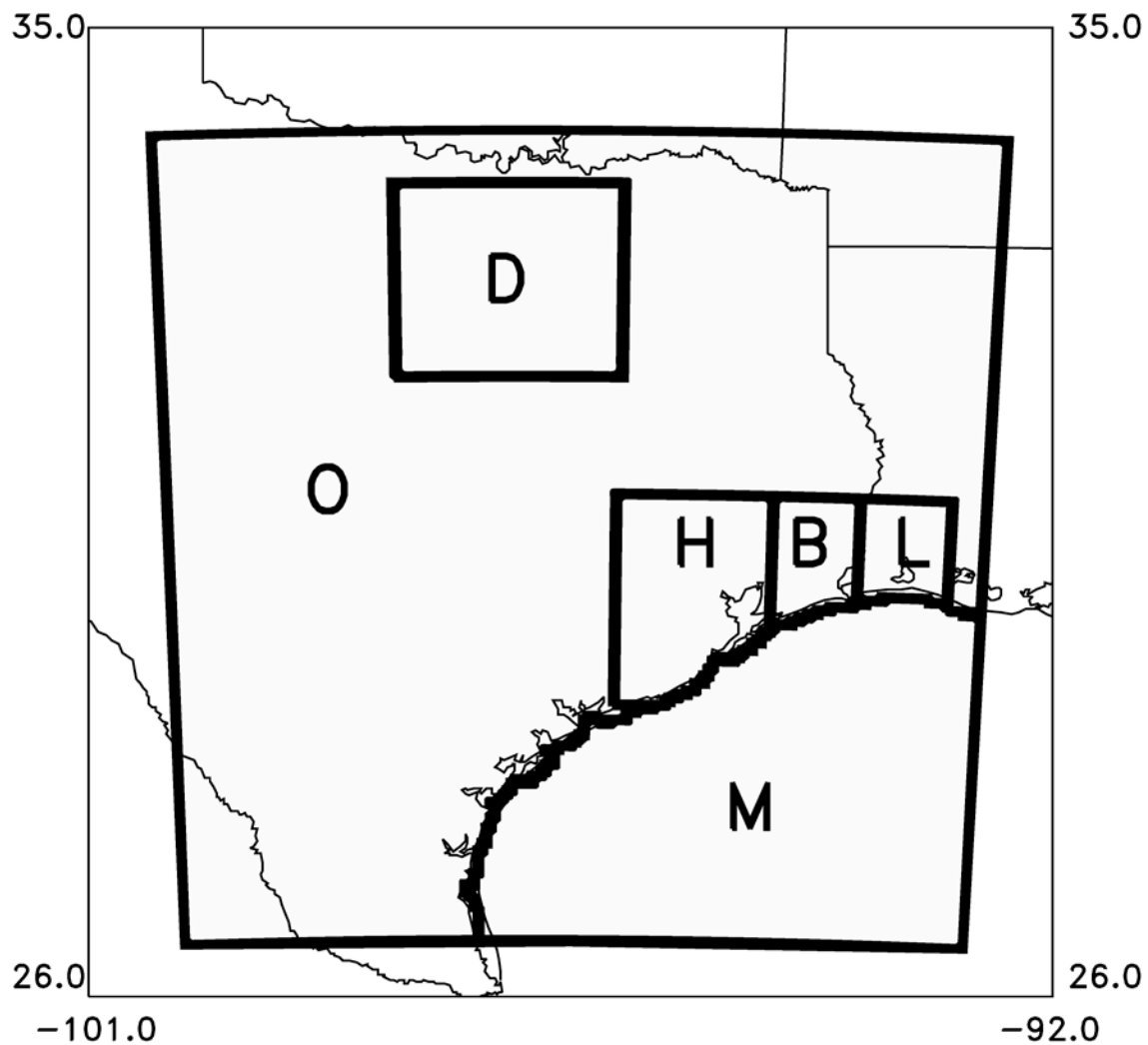


Figure 24. 4 km CMAQ domain showing the five anthropogenic source regions specified in the ozone source apportionment simulation (D=Dallas; H=Houston; B=Beaumont; L=Lake Charles; M=marine; O=other).

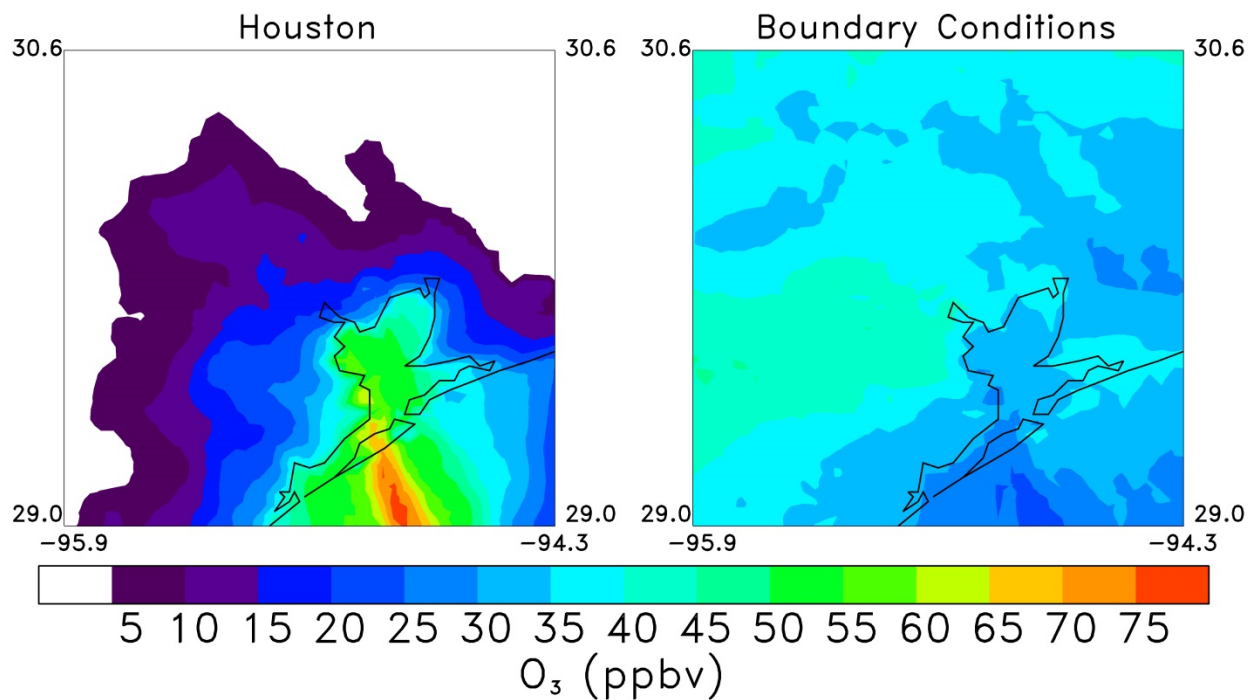


Figure 25. Amount of ozone that contributed to the maximum 8 hour average ozone on September 25, 2013 from anthropogenic emissions in the Houston source region (left) and boundary conditions (right).

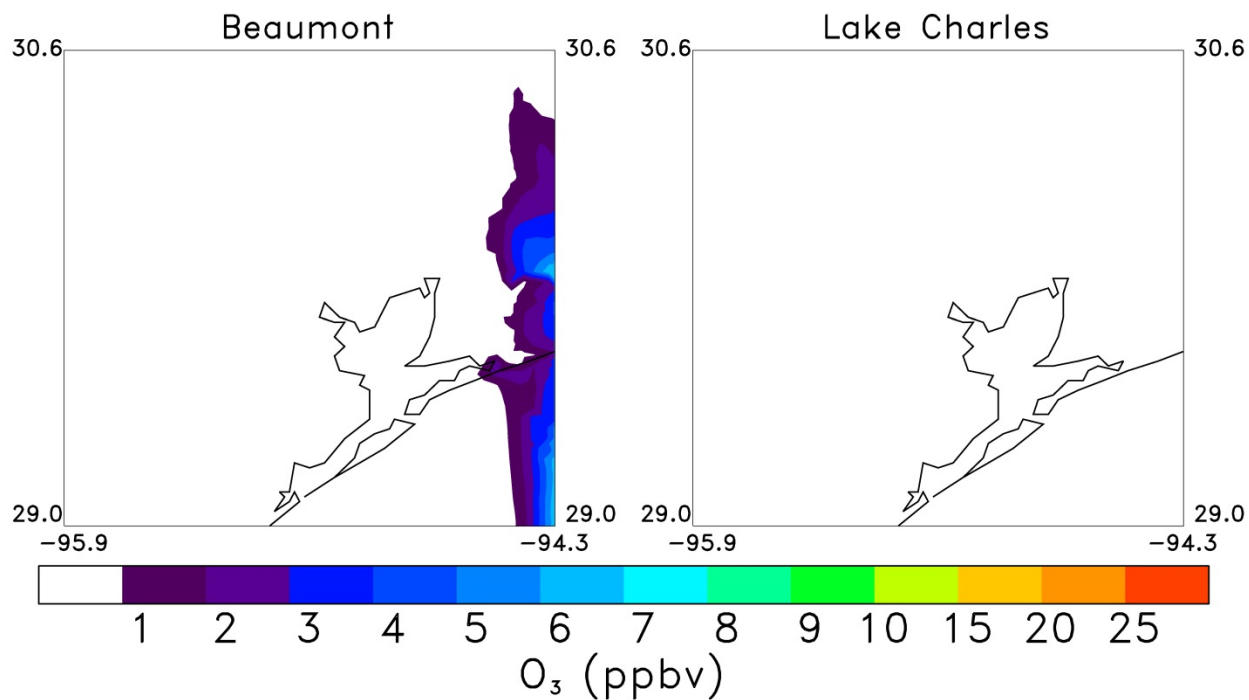


Figure 26. Amount of ozone that contributed to the maximum 8 hour average ozone on September 25, 2013 from anthropogenic emissions in the Beaumont source region (left) and Lake Charles source region (right).

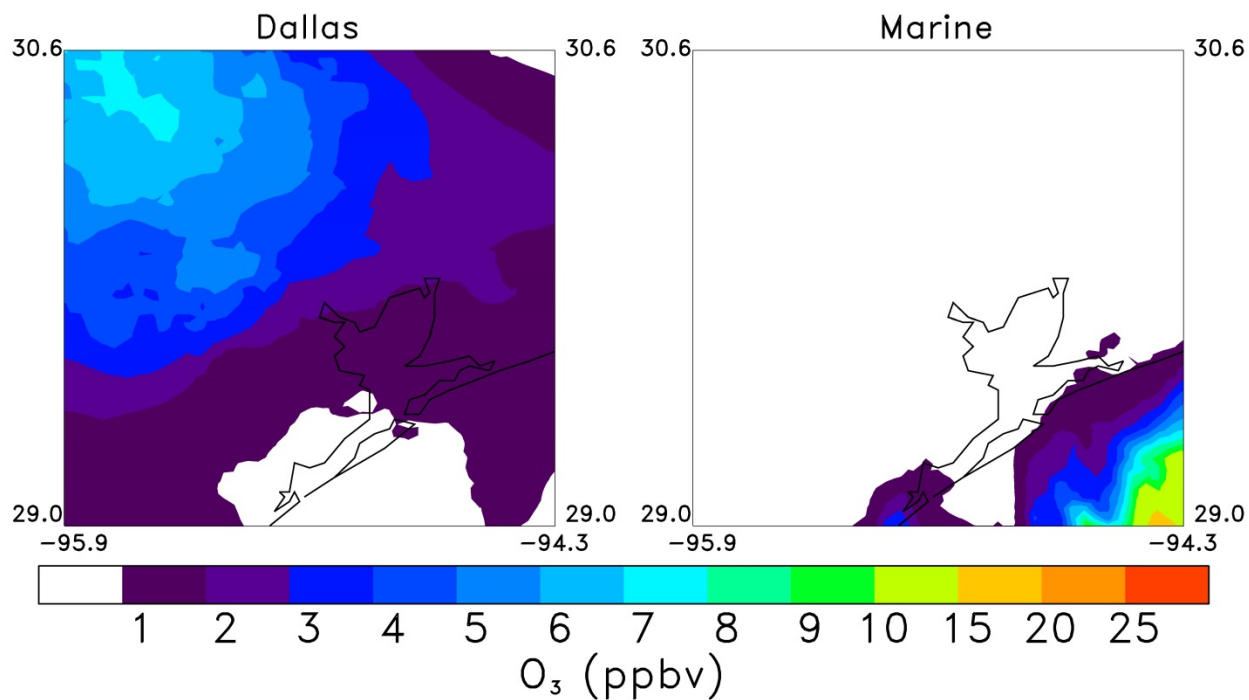


Figure 27. Amount of ozone that contributed to the maximum 8 hour average ozone on September 25, 2013 from anthropogenic emissions in the Dallas source region (left) and Marine source region (right).

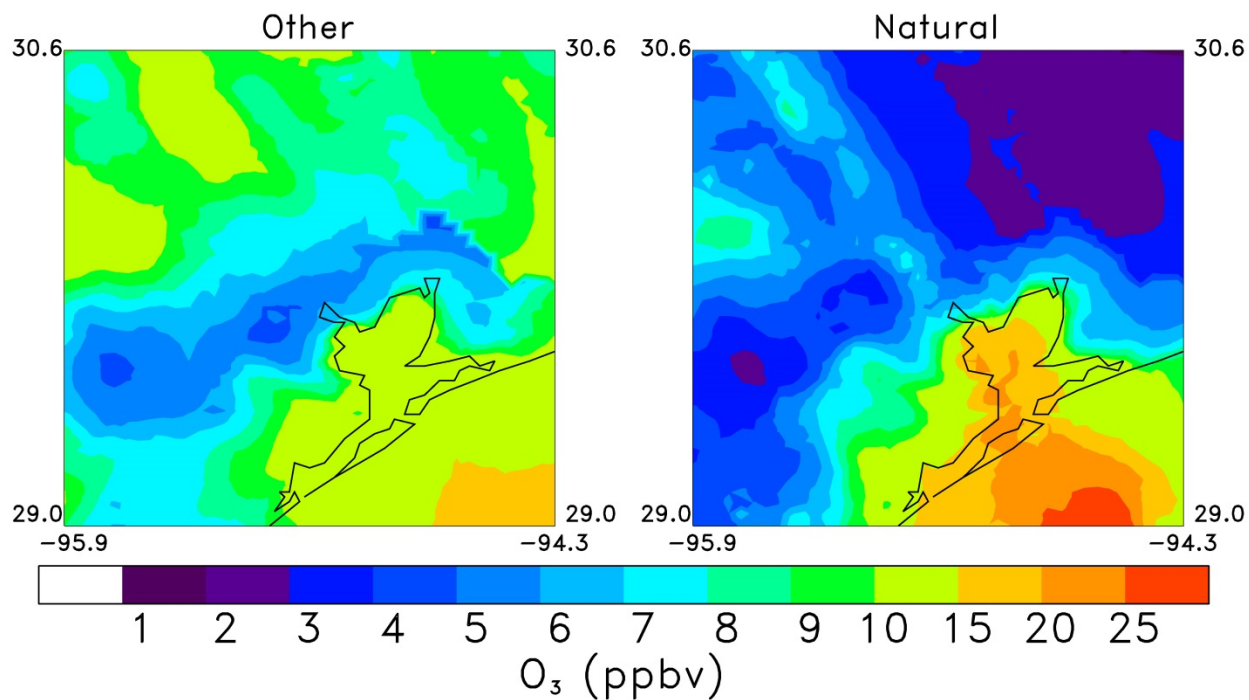


Figure 28. Amount of ozone that contributed to the maximum 8 hour average ozone on September 25, 2013 from anthropogenic emissions in the Other source region (left) and all natural sources (i.e., biogenic, lightning) within the 4 km domain (right).

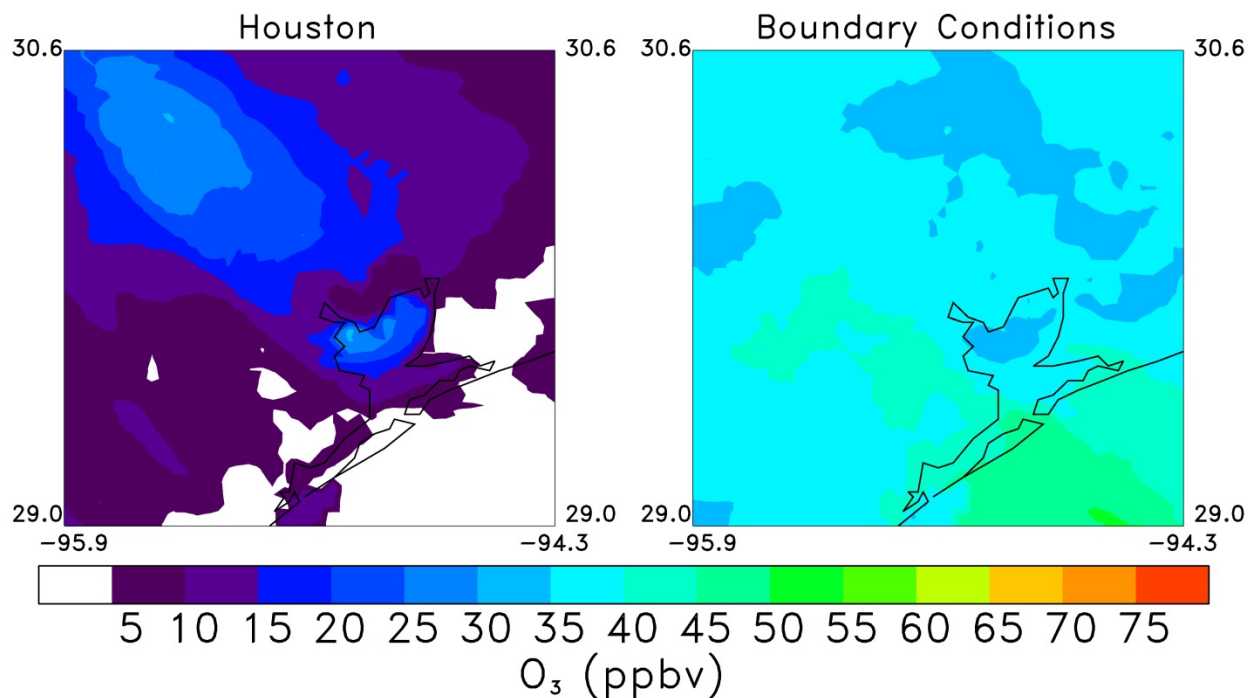


Figure 29. Amount of ozone that contributed to the maximum 8 hour average ozone on September 26, 2013 from anthropogenic emissions in the Houston source region (left) and boundary conditions (right).

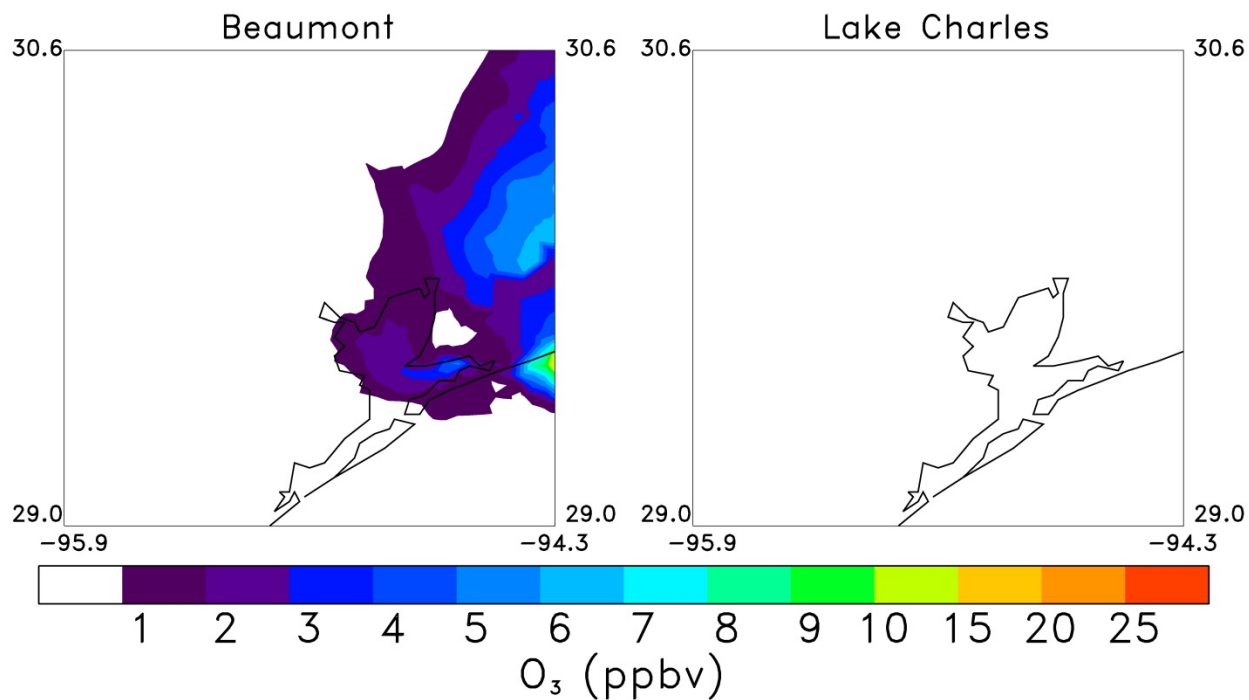


Figure 30. Amount of ozone that contributed to the maximum 8 hour average ozone on September 26, 2013 from anthropogenic emissions in the Beaumont source region (left) and Lake Charles source region (right).

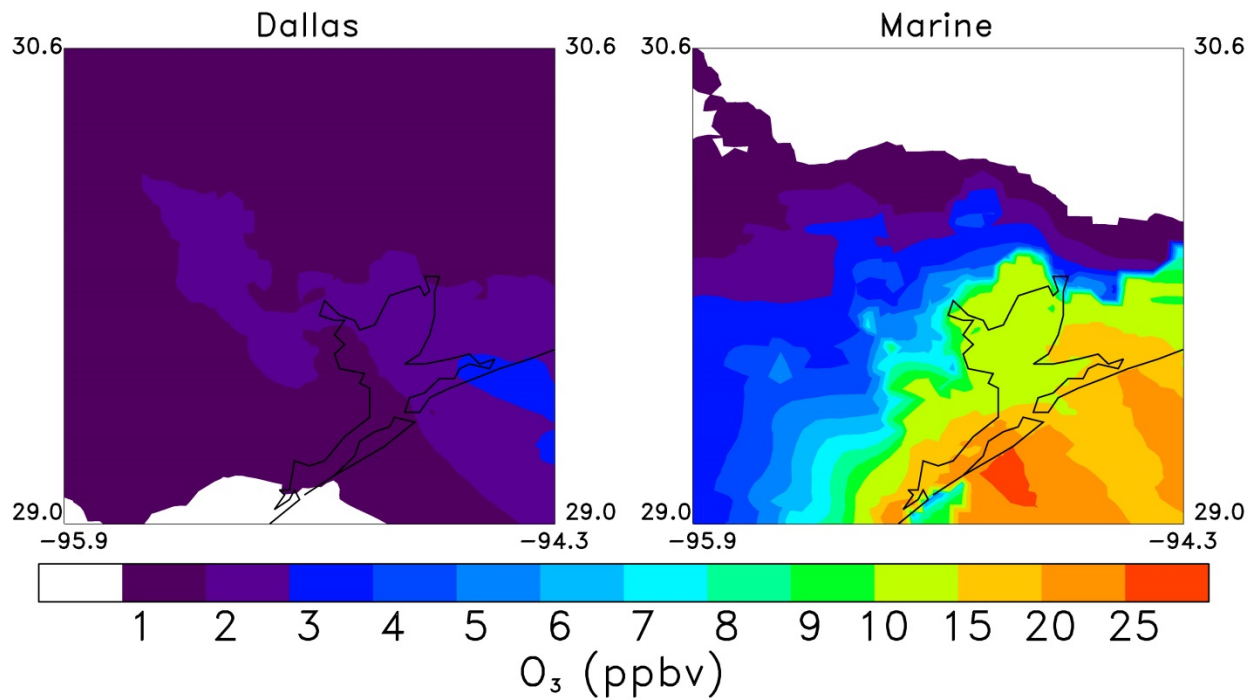


Figure 31. Amount of ozone that contributed to the maximum 8 hour average ozone on September 26, 2013 from anthropogenic emissions in the Dallas source region (left) and Marine source region (right).

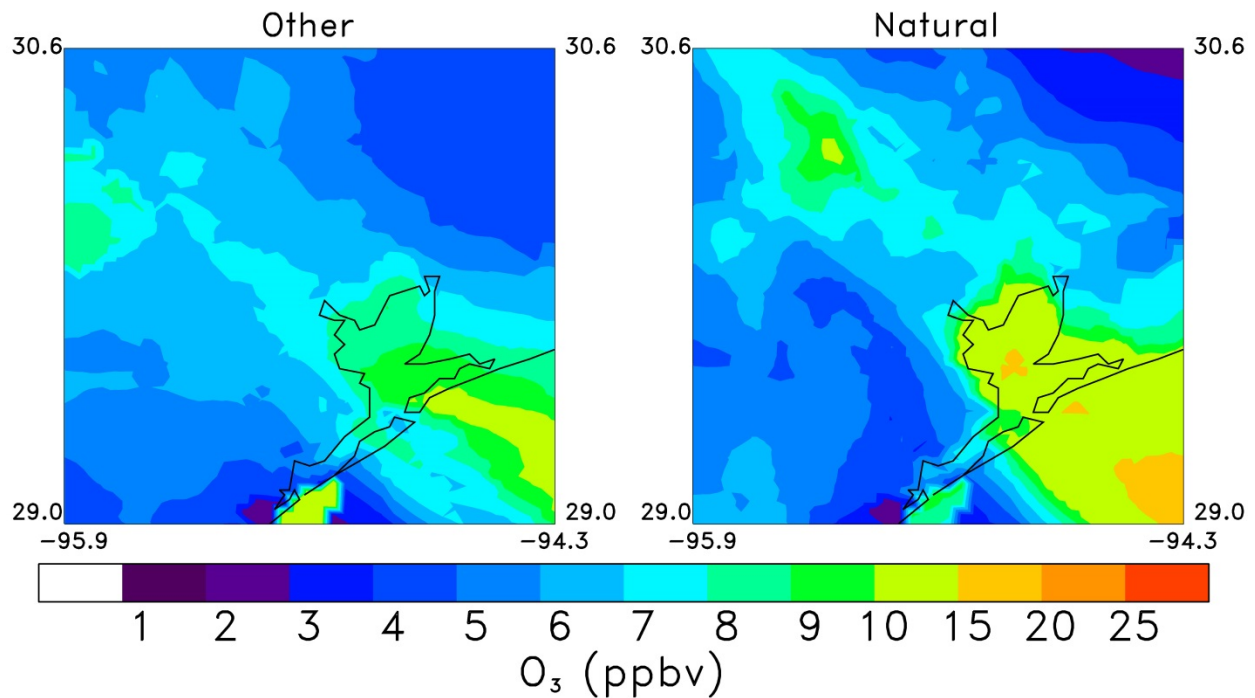


Figure 32. Amount of ozone that contributed to the maximum 8 hour average ozone on September 26, 2013 from anthropogenic emissions in the Other source region (left) and all natural sources (i.e., biogenic, lightning) within the 4 km domain (right).

Date	Observed	Model	Houston	Dallas	Beaumont	Lake Charles	Marine	Other	Natural	Boundary Conditions	Initial Conditions
25	124	84.85	26.95 (31.77)	1.74 (2.05)	0.05 (0.06)	0.05 (0.06)	0.11 (0.13)	6.96 (8.21)	9.47 (11.16)	40.00 (47.14)	0.50 (0.59)
26	79	81.80	14.81 (18.10)	1.99 (2.43)	0.59 (0.72)	0.11 (0.14)	9.44 (11.54)	7.93 (9.69)	8.71 (10.65)	38.43 (46.98)	1.28 (1.57)

Table 17. Observed and model simulated maximum 8 hour average ozone, contribution of maximum 8 hour average ozone (absolute value followed by percent contribution to model simulated amount in parentheses) from anthropogenic emissions in the Houston, Dallas, Beaumont, Lake Charles, Marine, and Other source regions, natural emissions throughout the 4 km domain, boundary conditions, and initial conditions at La Porte Sylvan Beach on September 25 and 26, 2013.

Date	Observed	Model	Houston	Dallas	Beaumont	Lake Charles	Marine	Other	Natural	Boundary Conditions	Initial Conditions
25	69	64.79	5.36 (8.27)	6.28 (9.69)	0.25 (0.39)	0.25 (0.39)	0.26 (0.40)	10.73 (16.56)	6.79 (10.48)	34.29 (52.93)	1.48 (2.29)
26	85	79.69	27.02 (33.91)	1.39 (1.75)	0.07 (0.09)	0.05 (0.07)	0.77 (0.97)	6.26 (7.85)	9.46 (11.87)	35.29 (44.29)	1.11 (1.40)

Table 18. Same as Table 17, but for Conroe.

Date	Observed	Model	Houston	Dallas	Beaumont	Lake Charles	Marine	Other	Natural	Boundary Conditions	Initial Conditions
25	89	73.70	17.39 (23.59)	3.24 (4.39)	0.14 (0.19)	0.15 (0.20)	0.23 (0.31)	5.58 (7.57)	4.65 (6.31)	42.24 (57.32)	0.64 (0.87)
26	65	70.97	10.91 (15.37)	2.16 (3.04)	0.08 (0.11)	0.07 (0.10)	4.95 (6.98)	6.94 (9.78)	5.13 (7.23)	40.22 (56.67)	1.17 (1.64)

Table 19. Same as Table 17, but for Park Place.

Date	Observed	Model	Houston	Dallas	Beaumont	Lake Charles	Marine	Other	Natural	Boundary Conditions	Initial Conditions
25	78	68.31	8.91 (13.04)	3.78 (5.53)	0.10 (0.14)	0.10 (0.15)	0.12 (0.17)	6.67 (9.76)	3.91 (5.72)	44.69 (65.42)	0.66 (0.96)
26	60	67.08	8.77 (13.07)	1.95 (2.91)	0.06 (0.09)	0.06 (0.09)	3.29 (4.91)	6.65 (9.92)	4.91 (7.32)	40.93 (61.02)	1.34 (2.00)

Table 20. Same as Table 17, but for Bayland Park.

5.0 SATELLITE ANALYSIS

We analyzed Ozone Monitoring Instrument (OMI) total ozone, OMI tropospheric NO₂, Moderate Resolution Imaging Spectrometer (MODIS) aerosol optical depth (AOD), and Measurement Of Pollution In The Troposphere (MOPITT) total column CO for the September 24-26 period (Figure 33 through Figure 44). No OMI or MOPITT data is available over the study

region on September 25. Most of the ozone in the total ozone column is in the stratosphere, so therefore it is a poor indicator for surface air quality; no indication of regionally transported lower tropospheric ozone is present in the OMI data. Tropospheric NO₂ values are between 2-4 molecules/cm² over East Texas and most of Louisiana on September 24 and 26. With just two images available for our study period, one on September 24 and another on September 26, we do not see a satellite signal indicating NO₂ was transported into Houston from a specific anthropogenic emissions source region. However, we do see higher tropospheric NO₂ values over the continent than over the Gulf of Mexico, suggesting that higher NO₂ concentrations are transported into Houston when transport is from the continent, which was the case during this episode. AOD values were low throughout the air pollution episode, which is not surprising since this was an ozone air pollution event, not a PM_{2.5} event (i.e., no exceedances in EPA's 24 hour average PM_{2.5} standard of 35 µg/m³ in and around Houston) and no elevated dust or fire plumes were observed over Houston by the NASA P-3B aircraft. There is no indication of regionally transported CO into Houston from a specific anthropogenic emission source region from the MOPITT instrument. The sparseness of MOPITT total CO observations, both spatially and temporally, makes it difficult to detect regionally transported pollution into Houston. However, like the tropospheric NO₂ columns, MOPITT CO reveals higher CO over the continent than over the Gulf of Mexico. Again, this suggests higher pollution levels are transported into Houston when transport is from the continent than from the Gulf of Mexico.

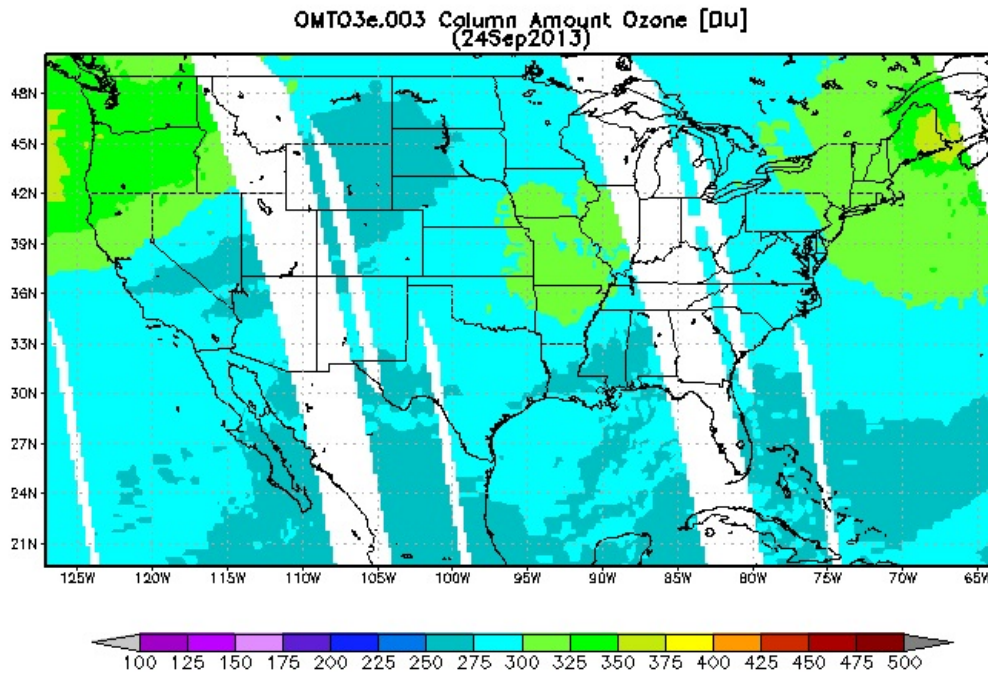


Figure 33. OMI total ozone column on September 24, 2013.

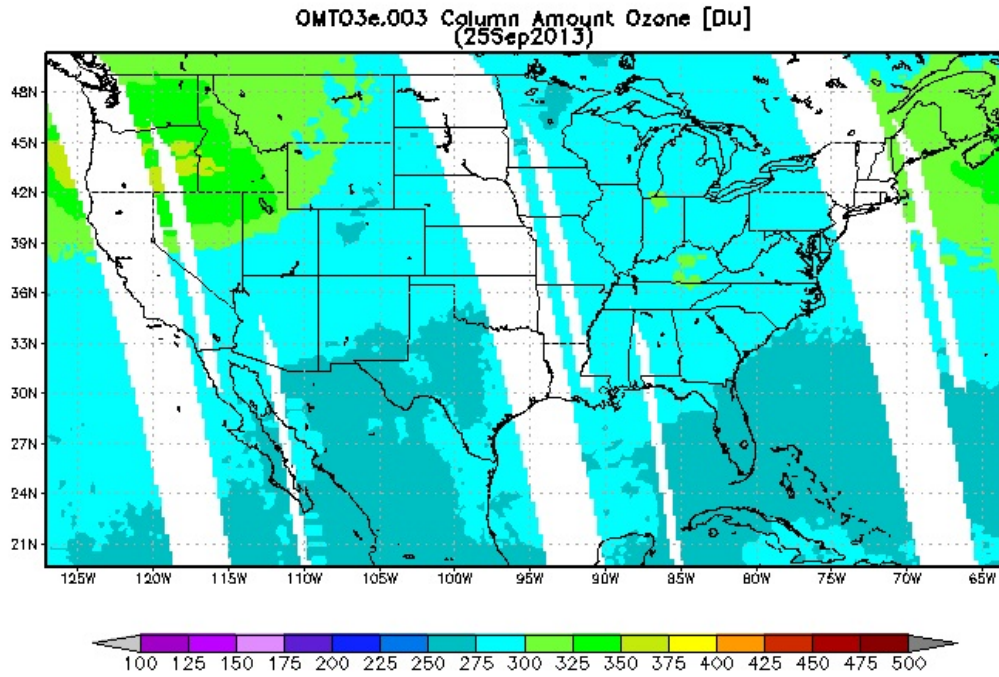


Figure 34. OMI total ozone column on September 25, 2013.

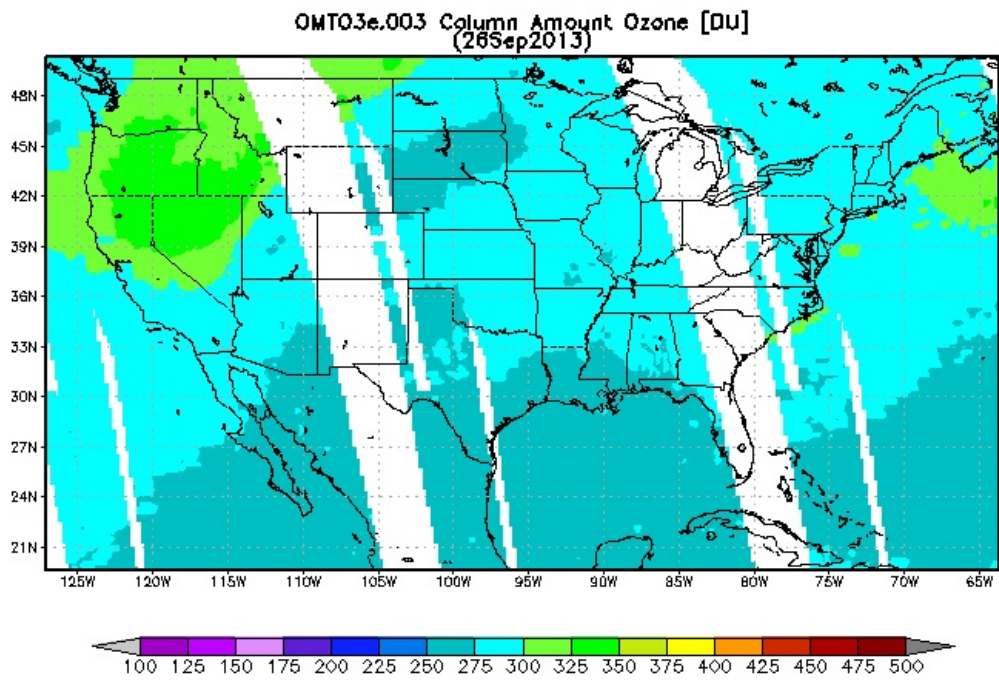


Figure 35. OMI total ozone column on September 26, 2013.

OMNO2d.003 NO2 Tropospheric Column Amount (Cloud-Screened at 30%) [10^{15} molec/cm 2]
(24Sep2013)

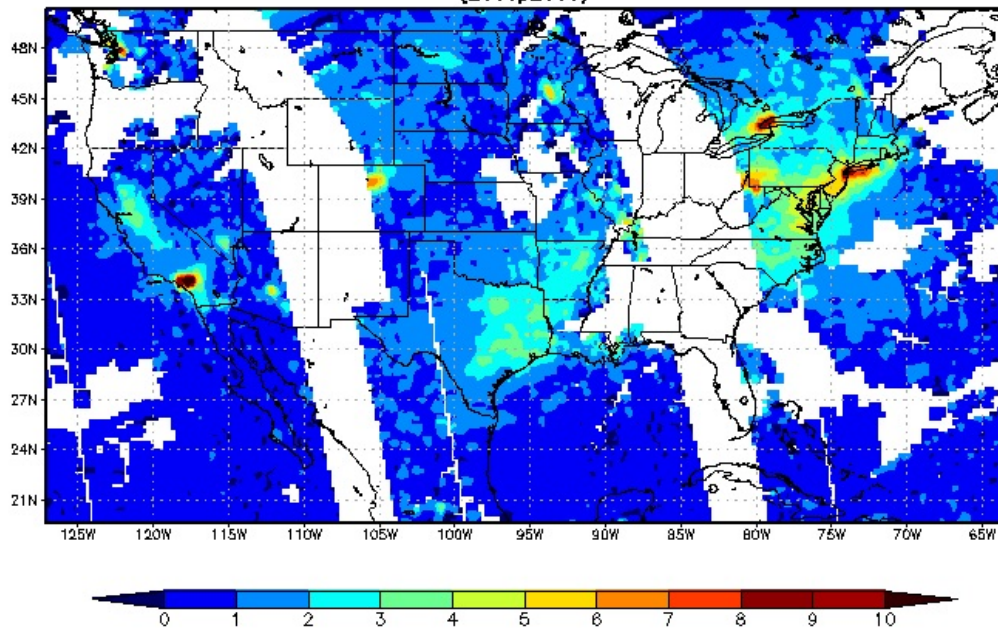


Figure 36. OMI NO $_2$ tropospheric column on September 24, 2013.

OMNO2d.003 NO2 Tropospheric Column Amount (Cloud-Screened at 30%) [10^{15} molec/cm 2]
(25Sep2013)

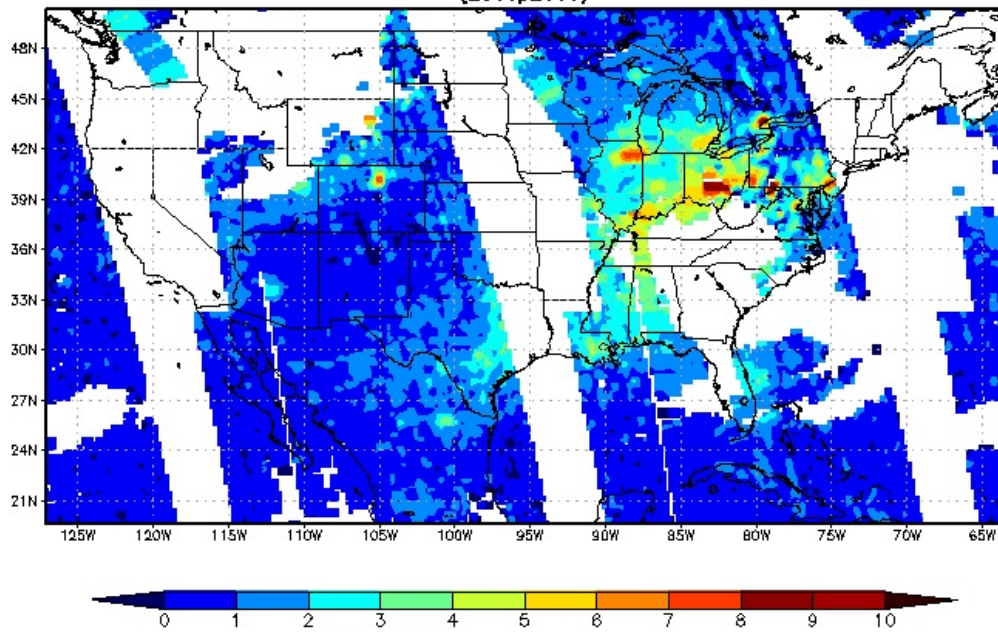


Figure 37. OMI NO $_2$ tropospheric column on September 25, 2013.

OMNO2d.003 NO2 Tropospheric Column Amount (Cloud-Screened at 30%) [10^{15} molec/cm²]
(26Sep2013)

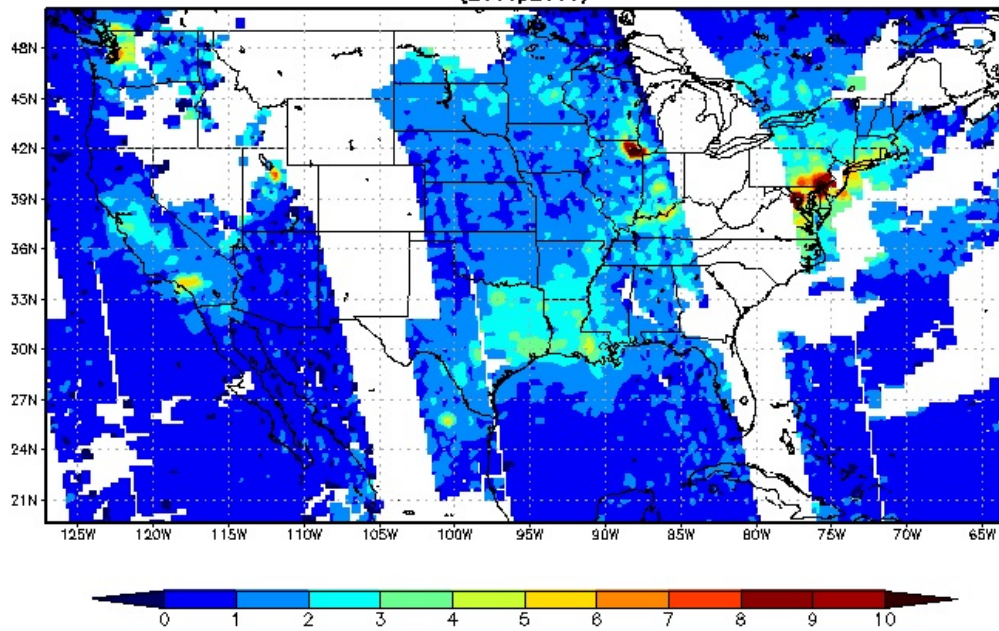


Figure 38. OMI NO₂ tropospheric column on September 26, 2013.

MOD08_D3.051 Aerosol Optical Depth at 550 nm [unitless]
(24Sep2013)

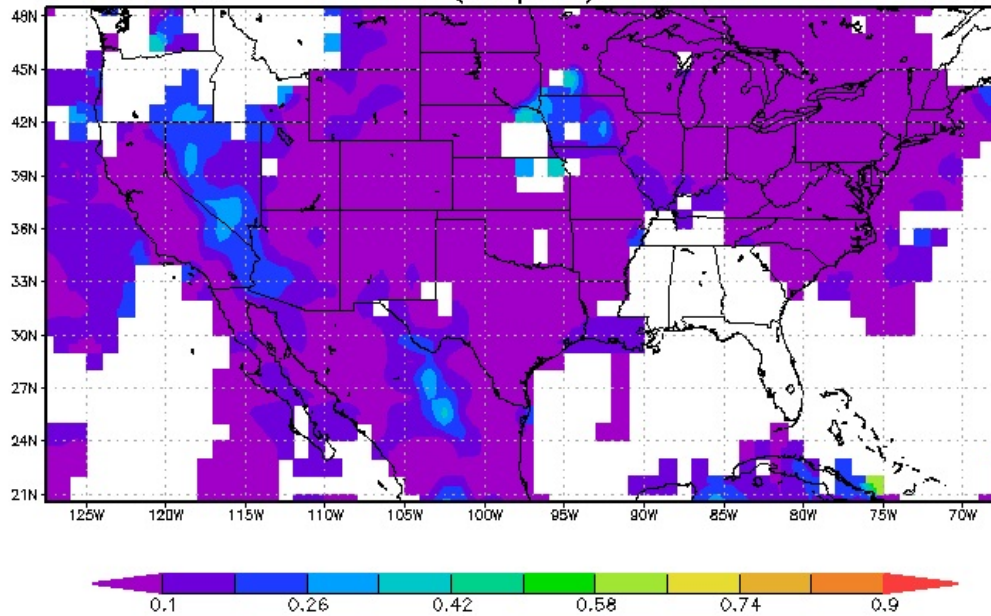


Figure 39. MODIS AOD on September 24, 2013.

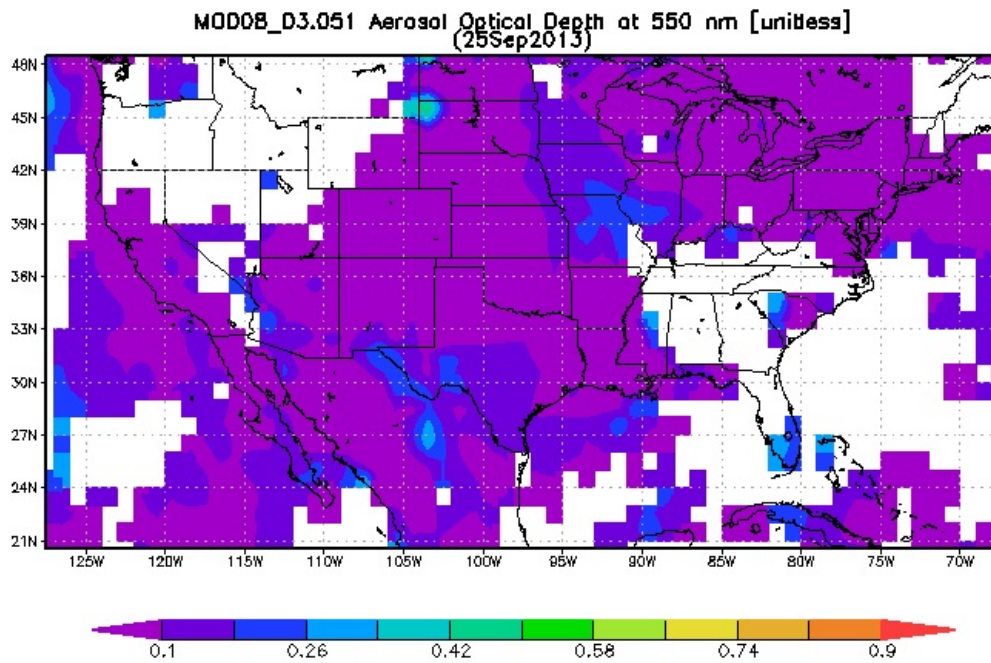


Figure 40. MODIS AOD on September 25, 2013.

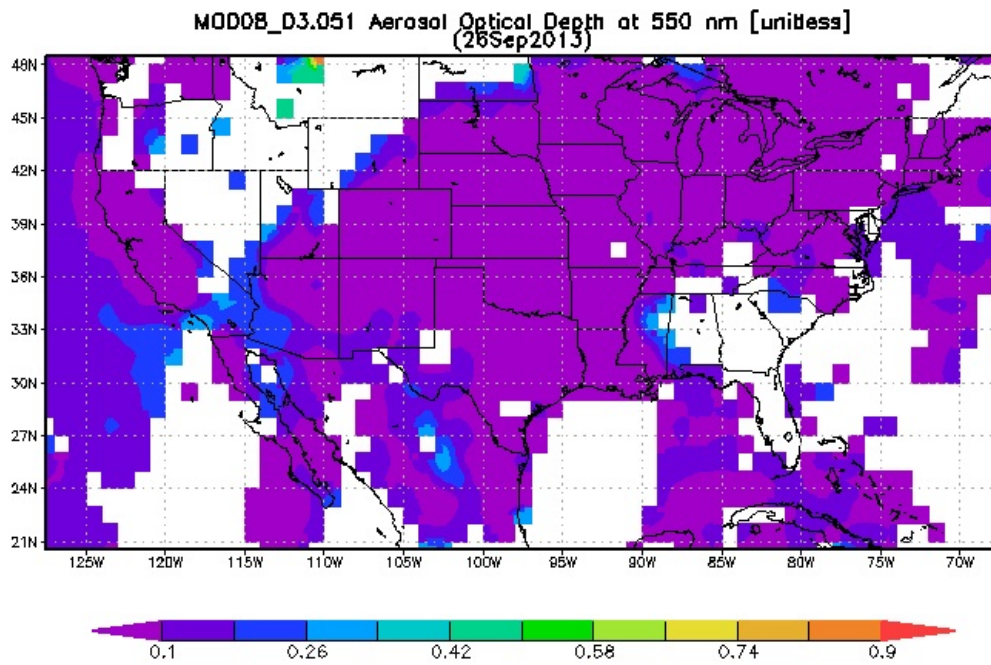


Figure 41. MODIS AOD on September 26, 2013.

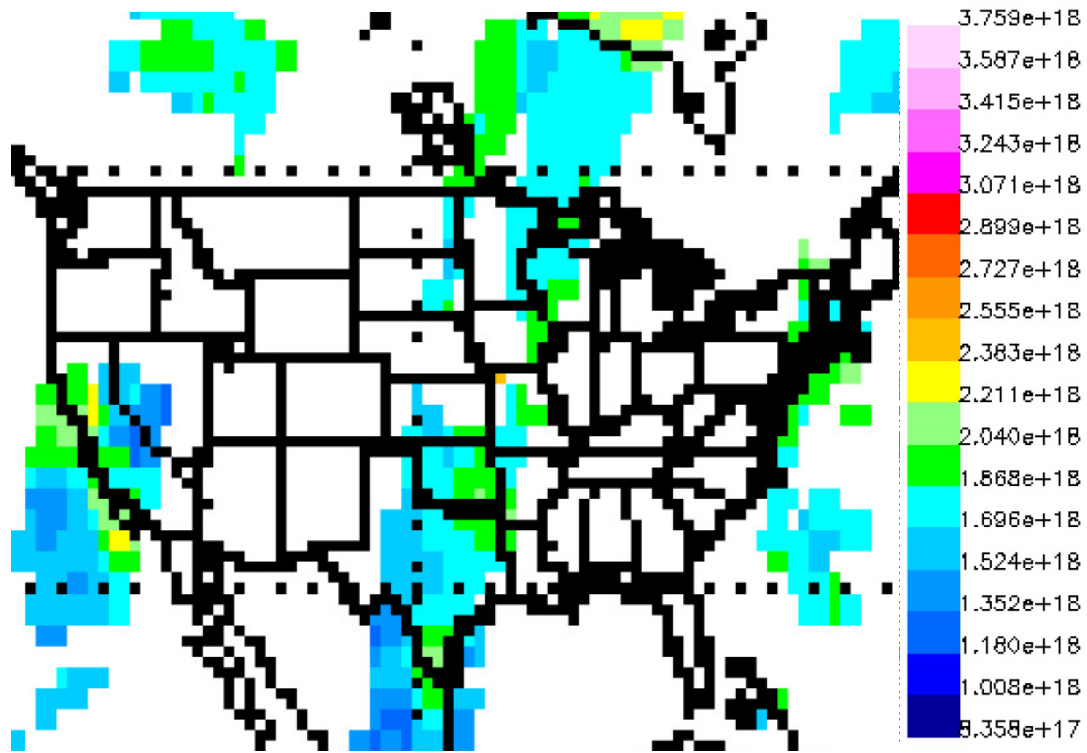


Figure 42. MOPITT total CO column on September 24, 2013.

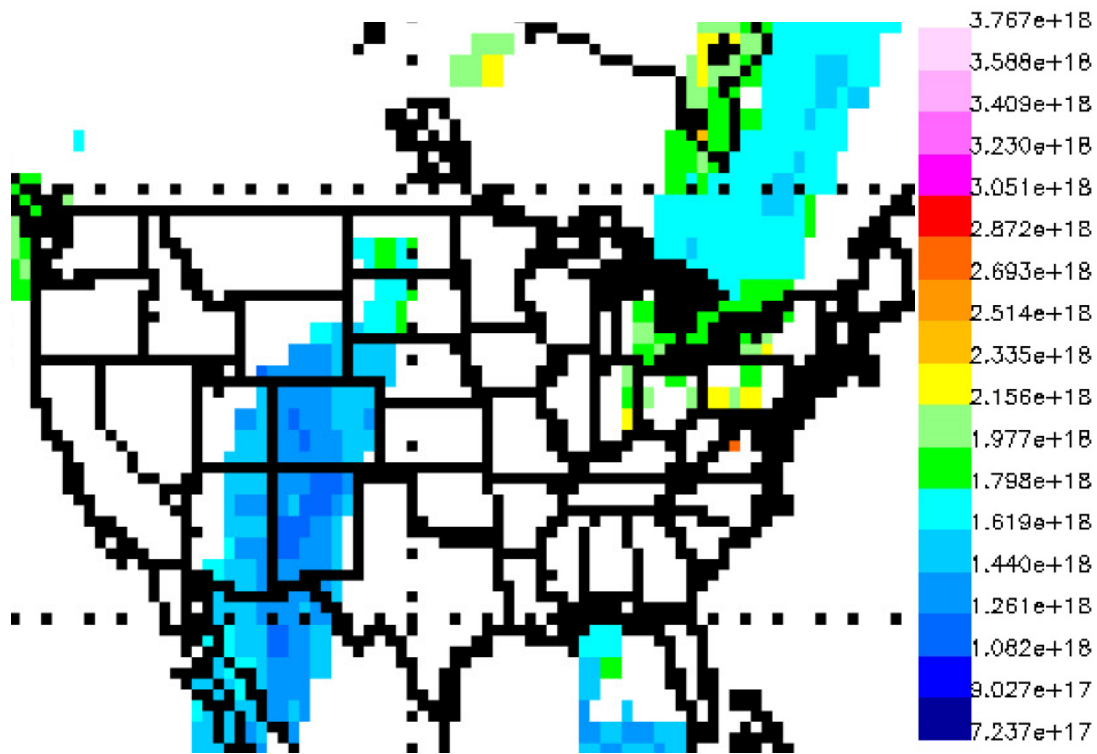


Figure 43. MOPITT total CO column on September 25, 2013.

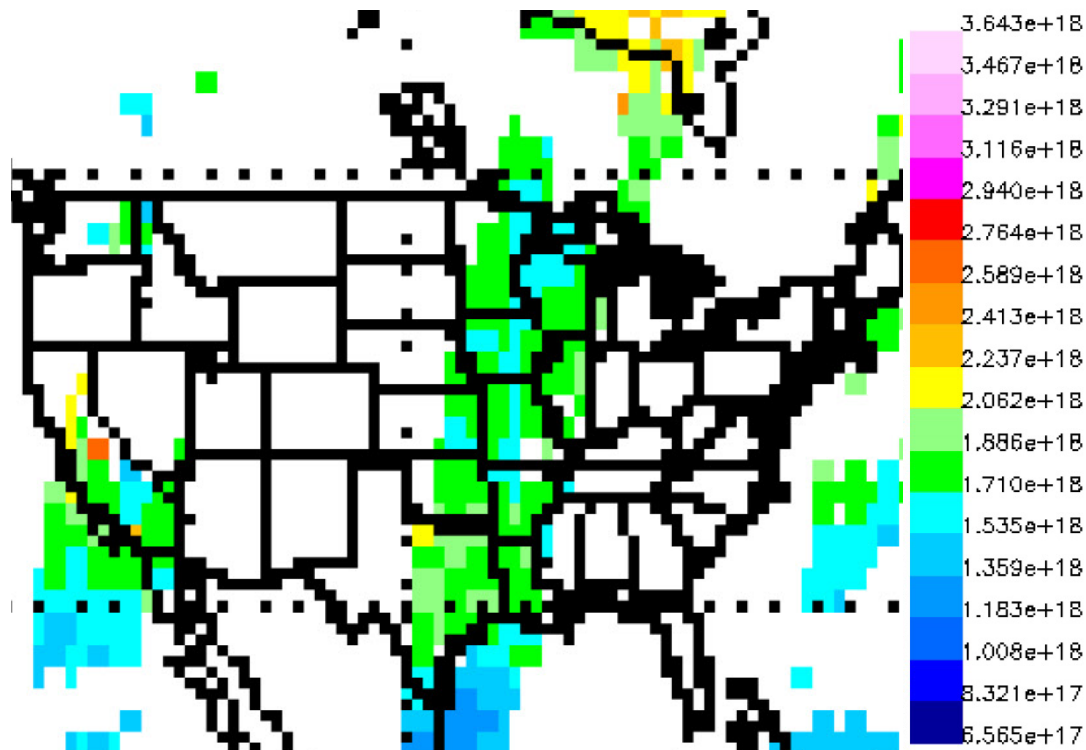


Figure 44. MOPITT total CO column on September 26, 2013.

6.0 AUDITS OF DATA QUALITY

More than 10% of the WRF and CMAQ model input and output files, scripts, and analysis products were reviewed for quality assurance purposes. Model inputs and outputs, model evaluation statistics, and graphics generated for this project are being stored and will continue to be for at least three years after the completion of the project at NASA GSFC. In addition, all model inputs, outputs, and post-processing analyses will be sent to the University of Texas after the completion of the project.

7.0 CONCLUSIONS AND RECOMMENDATIONS

7.1 Summary

We performed WRF and CMAQ simulations of the DISCOVER-AQ Houston, TX deployment and focused our evaluation on the largest surface ozone episode in Houston during 2013. Our initial WRF simulation performed poorly. WRF did not accurately simulate sea and bay breeze circulations on September 25. We modified our WRF inputs, set-up, and modeling technique to obtain improved results. Our improved WRF run utilized EPA's iterative technique and accurately simulated sea and bay breeze circulations on September 25. The 2nd iterative WRF run was used to drive an improved CMAQ simulation, which simulated a widespread area that exceeded the EPA ozone standard on September 25, which agrees with observations.

A statistical analysis was performed on the WRF and CMAQ simulations. The results show that the original 4 km and the 1st iterative 1 km WRF runs poorly simulated 10 m wind direction,

while little improvement is seen between the 1st and 2nd iterative 4 km WRF simulations. This suggests that the improved WRF modeling inputs, options, and technique upgraded the results and performing a 2nd iterative WRF simulation for the 1 km domain is necessary to obtain meaningful results. The CMAQ statistical evaluation using ground and aircraft ozone observations shows that little improvement was gained from adding a 1 km domain. However, the 1 km non-point anthropogenic emissions files were obtained by interpolating a 4 km emissions inventory. Therefore, we cannot definitively determine whether or not adding a 1 km domain will improve surface ozone model results over a 4 km domain.

A back trajectory analysis indicated that anthropogenic emissions from Houston, Dallas, Beaumont, Lake Charles, and marine areas may have influenced surface ozone on September 25 and 26. A CMAQ source apportionment simulation revealed that Houston anthropogenic emissions were the predominant contributor of anthropogenic emissions for this air pollution episode.

Satellite observations showed higher air pollution levels are present over the continent than the Gulf of Mexico. This indicates that higher air pollution concentrations are transported into Houston when transport is from the continent than from the Gulf of Mexico, which was the case during this air pollution episode.

7.2 Recommendations

Based on the project results, we suggest the following:

- Drive future WRF simulations with the 12 km NAM and perform observational and analysis nudging on all domains
- Perform a 2nd iterative WRF simulation for future runs for domains with very high resolution (1 km).

We suggest the following additional work:

- Run CMAQ or CAMx with source apportionment isolating various source sectors (i.e., on-road mobile, non-road mobile off-road mobile, area, point) to determine not only the impact of source regions on ozone concentrations, but also source sectors within each region.
- Run CMAQ and CAMx with a larger 4 km domain than used in this study to determine the source regions impacting air quality in Houston outside of the 4 km domain performed in this study.
- Test model performance of a 1 km horizontal resolution CMAQ model simulation with emissions input files created for a 1 km resolution domain (i.e., emissions not interpolated from a 4 km horizontal resolution domain);
- Evaluate CMAQ run with halogen chemistry (available in next release) to determine how much it improves the high ozone bias at Galveston.

8.0 REFERENCES

- Appel, K.W., R.C. Gilliam, J.E. Pleim, G.A. Pouliot, D.C. Wong, C. Hogrefe, S.J. Roselle, and R. Mathur, 2014. Improvements to the WRF-CMAQ modeling system for fine-scale air quality simulations, *EM*, September 2014, 16-21.
- Banta, R., C.J. Senff, J. Nielsen-Gammon, L. Darby, T. Ryerson, R. Alvarez, P. Sandberg, E. Williams, and M. Trainer, 2005. A bad air day in Houston, *Bulletin of the American Meteorological Society*, 86, 657-669, doi: 10.1175/BAMS-86-5-657.
- Chen, F., S. Miao, M. Tewari, J.-W. Bao, and H. Kusaka, 2011. A numerical study of interactions between surface forcing and sea breeze circulations and their effects on stagnation in the greater Houston area, *Journal of Geophysical Research*, 116, D12105, doi:10.1029/2010JD015533.
- Darby, L.S., 2005. Cluster analysis of surface winds in Houston, Texas, and the impact of wind patterns on ozone, *Journal of Applied Meteorology*, 44, 1788-1806, doi:10.1175/JAM2320.1.
- Emery, C., B. Tai, and G. Yarwood, 2001. Enhanced Meteorological Modeling and Performance Evaluation for Two Texas Ozone Episodes. Prepared for the Texas Natural Resource Conservation Commission, prepared by ENVIRON International Corporation, Novato, CA.
- Estes, M., S. Berlin, A. Langford, M. Dong, and D. Parrish, 2013. Trends in background ozone in Houston-Galveston, 1998-2012, presented at the 12th Annual CMAS Conference, Chapel Hill, NC.
- Parrish, D.D., D.T. Allen, T.S. Bates, M. Estes, F.C. Fehsenfeld, G. Feingold, R. Ferrare, R.M. Hardesty, J.F. Meagher, J.W. Nielsen-Gammon, R.B. Pierce, T.B. Ryerson, J.H. Seinfeld, and E.J. Williams, 2009. Overview of the Second Texas Air Quality Study (TexAQS II) and the Gulf of Mexico Atmospheric Composition and Climate Study (GoMACCS), *Journal of Geophysical Research*, 114, D00F13, doi:10.1029/2009JD001842.
- Sarwar, G., B. Gantt, D. Schwede, K. Foley, R. Mahur, and A. Saiz-Lopez, 2015. Impact of enhanced ozone deposition and halogen chemistry on Tropospheric ozone over the Northern Hemisphere, *Environ. Sci. Technol.*, 49 (15), pp 9203-9211, doi:10.1021/acs.est.5b01657.
- Smith, J., F. Mercado, M. Estes, 2013. Characterization of Gulf of Mexico background ozone concentrations, presented at the 12th Annual CMAS Conference, Chapel Hill, NC.